Universitatea
Transilvania
din Brașov

INTERDISCIPLINARY DOCTORAL SCHOOL

Faculty of Mechanical Engineering

Iuliana TUDORACHE (COSTIUC)

OPTIMIZING THE PRESSURE WAVE SUPERCHARGER DESIGN FOR EXTENDED APPLICATION

ABSTRACT

Scientific coordinator

Prof. Anghel CHIRU, PhD

BRAȘOV, 2022

CONTENTS

FORWORD

The internal combustion engine is still an important research topic due to its indispensable role in modern society to meet its transportation and energy needs. Indeed, the improvement in the quality of life and work thanks to the thermal engine is considerable, but so are the unpleasant effects we face today: pollution or global warming. Therefore, car manufacturers are interested in launching vehicles with propulsion systems that use more environment "friendly" fuels, or hybrid or electric models. Legislated standards on emissions force manufacturers to implement new, efficient technologies, thus, these new, improved powertrains will require new auxuliary equipment to increase or maintain the overall performance of engines whose production is becoming limited. SUPercharging is one of the methods of increasing engine performance and reducing emissions, a technology that requires constant improvements and reconfigurations. A 100-year-old SUPercharging technology is the pressure wave technology. The operation of the pressure wave SUPercharger (PWS) is based on the transfer of the energy contained in the exhaust gases to the intake air, using the properties of pressure waves to change the parameters of the fluid through which they propagate. The objectives of this thesis refer to the optimization of the PWS configuration by: improving the geometric shapes and sizes of the rotor starting from the conventional PWS CX-93, designing a new SUPercharger with modified geometry, reduced dimensions and noise, with the aim of expanding the range of applicability of the new PWS to engines that respond to current performance and emissions trends.

In accomplishing of this thesis and in my professional development, I had the honor of being helped and guided by personalities in the field and, at the same time, people of a special human quality, to whom I thank with deep gratitude. I would like to thank, first of all, Prof. Anghel Chiru, my scientific SUPervisor, who offered me valuable suggestions and precious methodological guidelines. I also want to thank the guiding professors: Prof. Gheorghe-Alexandru Radu, Prof. Corneliu Cofaru, Prof.Nicolae Ispas, for the pertinent advice and help offered, as well as to my colleagues from the Department of Automotive and Transport Engineering who constantly encouraged me in this endeavor. I also thank the students who constantly challenged me to at least live up to their enthusiasm and joy when proceeding on a new life path. I also thank the Vlahia family, who offered me a particularly beautiful space to create, write or regain my energy and courage. I would like to thank my parents and my brother and, last but not least, my daughter Iulia, who encouraged me with unwavering confidence, and my husband, Liviu, who always knows how to create the perfect space in which I can express my whole potential.

Braşov, 2022 Iuliana Costiuc

CHAPTER 1| THE ACTUALITY OF THE TOPIC. THESIS OBJECTIVES

1.1 INTERNAL COMBUSTION ENGINES. THEIR ROLE IN TODAY'S WORLD.

The dependence of modern society on transport and energy places the internal combustion engines still under the attention of researchers, who are mainly targeting the improvement of performance and design, as well as the optimization of their energy and ecological management, together with the significant decrease of polluting emissions of gases with greenhouse effect. Indeed, without the internal combustion engine, the world as we know it today would function quite differently! The improvement in the quality of life and work due to the existence of the thermal engine is considerable, as are the unpleasant effects we are facing today, with long-term consequences on our planet: pollution or global warming. Therefore, car manufacturers are interested in launching vehicles with propulsion systems with improved performance but with reduced emissions, introducing in recent years new models that use alternative or low-carbon fuels, hybrid or electric models.

The thermal engine has a history of more than three centuries, evolving from its primitive "relative" - the internal combustion piston engine using gunpowder as fuel, suggested by Jean de Hautefeuille in 1678 [1] and prototyped by Christiaan Huygens in 1680 [2] – up to the highly computerized and technologically advanced contemporary engines. The first internal combustion engines as we know them today were developed beginning in the second half of the 19th century and were soon used for transportation; later they made possible the development of the automotive, marine and aviation industries or the production of electricity. Currently, the development of the field of transport has led to an explosive increase in the number of vehicles that use the fossil fuel burning engine as a propulsion system and, implicitly, in pollutant and greenhouse gas emissions. One of the main concerns of mankind refers to the increase in the average global temperature on the planet and the long-term negative consequences of this phenomenon. Therefore, the European Union has adopted restrictive legislation in the field of propulsion systems – for example, the EU has set as a priority objective for 2030 a 55% reduction in greenhouse gas emissions compared to 1990 [5]. The most targeted greenhouse gas is carbon dioxide, the main source of its production being the road transport sector [6], so internal combustion engines have become the point of interest in terms of reducing emissions, as well as the efficient use of energy.

The global vehicle fleet currently exceeds 1 billion units [7], with a constant rapid growth that predicts that by 2036 the number of vehicles worldwide will reach approx. 2.8 billion units. Electric vehicles have gained more and more ground in the last decade, their number increasing from almost zero in 2010 to over 10.2 million in 2020 [7], with electric or plug-in hybrid vehicles reaching 4.6% of the total car sales in 2020.

The evolution of the car manufacturing industry [7] is presented in Figure 1.1, observing a considerable decrease during the economic crisis of 2009 and in 2020, when automobile production was strongly affected by the COVID-19 pandemic.

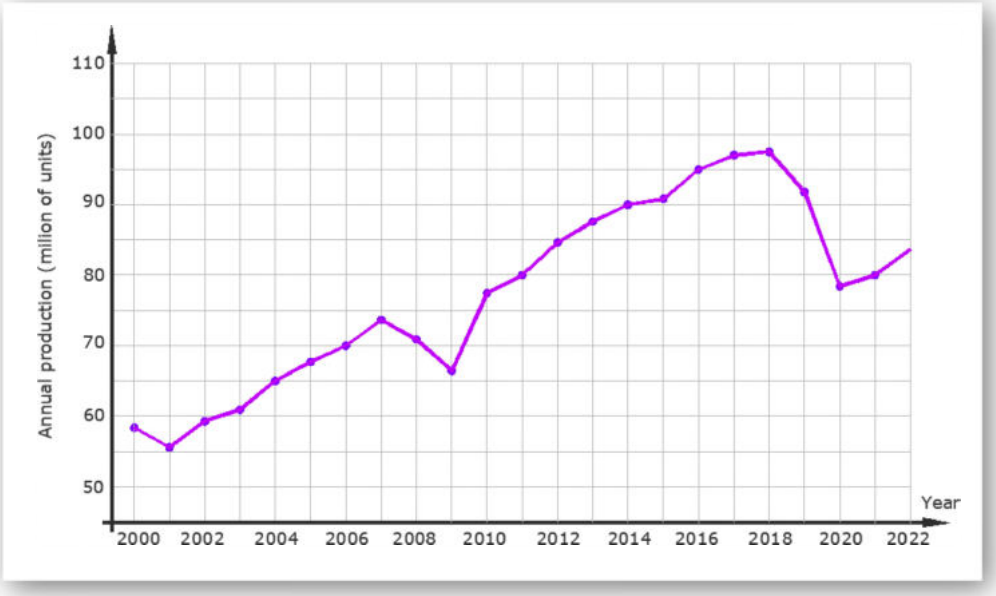

Figure 1.1 – Evolution of the vehicle manufacturing industry (made according to data from [7])

1.2 EMISSIONS – FORECASTS, TRENDS, SOLUTIONS

The policies aiming fossil fuels propulsion systems have become increasingly restrictive, both for heavy and light vehicles. The harmful effects of polluting agents on the environment and on the health of the population have attracted a tightening of European legislation regarding the permitted amounts of greenhouse effect elements or air pollution. Also, the change in the method of testing and measuring the emissions of light vehicles from NEDC (New European Driving Cycle) to WLTP (Worldwide harmonized Light vehicles Test Cycle), implemented since September 2017, changed the recorded values of energy consumption and vehicle emissions, which had a certain impact on the development strategy of car manufacturers, who stopped the production of some models and promoted or implemented models with reduced emissions [11], more "friendly" ecologically and energetically. In 2025-2030, significant changes are about to be made in the EU legislation regarding CO_2, with a 15% ... 30% reduction in CO_2 emissions [13]. Thus, car manufacturers have to make improvements to both the vehicle (through aerodynamics, rolling resistance, materials used, etc.) and the propulsion system [14]. Also, auxiliary equipment SUPpliers will be forced to raise its performance to help improve vehicle powertrain efficiency.

In conclusion, measures are needed in order to reduce emissions, including: the introduction of alternative propulsion technologies - hybrid or full-electric; eco-innovation – redesign, use of new materials and optimization of the design of auxiliary equipment and systems; improving the efficiency of

conventional engines; the implementation of new efficient technologies for the exhaust gas filtration system, etc. Improved systems based on the internal combustion engine therefore require new equipment or technologies to increase or maintain overall performance compared to engines whose production is becoming limited or eliminated.

1.3 THE PURPOSE OF THE WORK

Among the methods of achieving the desired goals described above are the new technologies introduced in the field of internal combustion engines (ICE), but also the methods of improving and increasing the performance of the existing ones. SUPercharging is one of the methods that offers the possibility of improving the operation of ICEs, but also of reducing emissions and polluting factors. A technology with a maximum potential yet untapped in SUPercharging is the pressure wave technology, and the equipment that implements this technology for ICE is the pressure wave compressor (supercharger) (PWS).

The need for continuous study and optimization of the equipment that facilitates the increase in engine performance is also supported by the current requirements regarding the emissions of greenhouse gases and pollutants of existing or future thermal engines. Although the current legislation tends to completely eliminate diesel engines, an idea justified by the specific pollutant emissions, its high performances will not be easily surpassed. Obviously, current research must be directed towards the implementation of innovative ideas for less polluting systems, being able to concretely justify the elimination of diesel engines from the world's vehicle fleet.

The present thesis aims to optimize one equipment used to increase the performance of the thermal engine, more precisely the design of the SUPupercharger, so that it can be used on engines that meet the current energetic and ecological requirements. The pressure wave technology presents some undeniable advantages over other PWS supercharging methods, including robustness, quick response over the entire engine speed range and lower manufacturing costs compared to the more efficient methods of recent years, such as turbocharging.

1.4 OBJECTIVES OF THE THESIS

The objectives of the current work concern bringing in foreground and highlighting the potential of the pressure wave supercharger, an equipment that, although it aroused the interest of researchers for several decades, reached the peak of interest before the development of the computed fast work, being thus marginalized due to the difficulty of writing and solving the equations that govern the complex phenomena inside it. However, because of the undisputed advantages of such an equipment, it has remained permanently in the attention of engineers in the aeronautical industry. Recently (2022), there has been a revival of the pressure wave supercharger through the contribution of Antrova GmbH, the

company that currently holds the Comprex patent. This paper aims to optimize the configuration of the Comprex CX-93 pressure wave supercharger, the most successful model made to date, fitted together with the 2.0-liter engine on the Mazda 626, sold in over 150,000 units. Therefore, the objectives of the paper can be stated as follows:

1. improving the dimensions and geometric shapes of the rotor channels of conventional PWS CX-93, by creating mathematical calculation models for the constitutive elements of the rotor;

2. the design of a new supercharger, symbolically named PWSMG (pressure wave supercharger with modified geometry) with an optimized configuration and reduced dimensions, with the aim of allowing:

3. widening the range of applicability of the new supercharger to "modern" engines, in line with current trends in the automotive industry (downsizing, eliminating diesel engines and developing engines using "environmentally friendly" fuels);

4. providing additional energy to the PWSMG shaft;

5. maintaining the energy transfer efficiency of the new supercharger at least at the level of the conventional one;

6. noise reduction compared to conventional Comprex.

1.5 STRUCTURE OF THE THESIS

In order to achieve the proposed objectives, the work was structured in several chapters, including generalities, history, basic theoretical notions, mathematical modeling, operation simulation, results and discussions, final conclusions and original contributions. Therefore, in the introductory Chapter 1, some of the current problems specific to propulsion systems based on the burning of fossil fuels were presented, the main « nerve point » being, without a doubt, the polluting emissions or those with a greenhouse effect, which have a particular impact on nature, life and biodiversity on the planet. In addition, the main solutions and perspectives in reducing the volume of emissions were stated, with an emphasis on the legislation of European or world standards imposed, especially in the field of transport, the main source of greenhouse gas emissions. The need to research systems for improvement of the performance of propulsion systems, with reference to the supercharging of internal combustion engines, was justified, thus outlining the objectives and purpose of this work.

Chapter 2 introduces supercharging technology and its benefits to internal combustion engines, and also highlights pressure wave technology as an alternative to classic supercharging systems. At the same time, a brief history of approximately one hundred years of research and development of the concept of a pressure exchanger with the role of a supercharger is presented. The principles of the operation and peculiarities of PWS, as well as the performance characteristics achieved with its use in the

automotive industry are presented in detail in Chapter 3, the purpose being to highlight the limits of use and performance of conventional PWS, as well as the benefits and shortcomings of the implementation of such a technology.

The objectives of this paper include the optimization of the geometric configuration of the PWS rotor and this objective involved the development of mathematical models for configuring the dimensions and geometry of the CX-93 rotor and the redesign of some of its elements, models presented in Chapter 4 of the thesis. It is configured as such: the shape and section of the channels, changing the number of channels or the number of rows of channels, tilting the axial direction of the rotor channels after an elliptical generator and reducing the length of the rotor accordingly. The preliminary evaluation of the new geometry was achieved by developing a calculation model for the pressure losses of the classic CX-93 and the 3 proposed variants, under simplified working assumptions. The calculations were initially made for the supercharger with modified geometry (PWSGM) without the axial inclination of the channels and the length of the rotor equal to that of the CX-93. Later, after the completion of the new geometry, the pressure losses were calculated after changing the length and axial direction of the channels. The description of the flow equations and the wave theory was carried out in the same chapter, detailing the models both for the pressure waves propagating inside the PWS channels, as well as for normal shock and oblique waves. The verification of the subsonic flow was achieved by creating a mathematical model for calculating the critical section and the maximum flow by analogy of the flow from the ports towards the rotor channels with the flow through convergent-divergent nozzles. The modeling of the virtual experimental stand used for experimental research in a virtual environment was presented at the end of this chapter.

The operation simulation and experimental validation of the new PWSGM was carried out using the previously configured AVL virtual model and the methodology and results were presented in Chapter 5. The AVL Boost virtual test rig used to simulate the operation of the PWSGM was initially configured to validate the model by simulating the operation of the real CX-93, starting from the input data reported in the specialized literature and obtained through real experimentation (the input data were presented in the Appendix 1), comparing them with the data from the literature, after which the new configuration of the PWSGM was set on the test rig previously used for the CX-93, followed by the simulation of the operation and the collection of results. The output data was analyzed in the same chapter, by checking the data imposed by the research hypotheses and by comparative analysis with real reported data.

In Chapter 6, the proposed objectives and the way in which they were achieved are reiterated. Also, the elements of originality and personal contributions of the author are detailed, followed by final conclusions and future research directions.

CAPITOLUL 2 | SUPERCHARGING WITH PRESSURE WAVE | HISTORY. MODE OF OPERATION. PERFORMANCES

2.1 GENERALITIES

Optimizing the operation of the internal combustion engine must refer in particular to its performance parameters: effective power, engine torque, fuel consumption and efficiency, as well as to ecological parameters: noise and emissions, and last but not least to costs, reliability and durability – maintenance requirements that influence operating costs. The processes that characterize the operation of an internal combustion engine are, in general, influenced by: constructive factors, the parameters of the gas exchange processes and the characteristic parameters of the operating and adjustment regime. These multiple influences on the operation of the internal combustion engine led to as many ways to improve the energy and ecological management of the ICE. Among these, supercharging is one of the most usual solutions developed and implemented by the constructors of propulsion systems for vehicles.

2.2 SUPERCHARGING

Supercharging is one ways to increase the power and efficiency of an engine, consisting of raising the pressure of the intake air with the aim of forcing a larger quantity containing more oxygen available for combustion to enter the cylinders each cycle. Increasing the intake air pressure can be achieved with a mechanical compressor driven from the crankshaft or a separate motor (mechanical supercharging) or by using the energy contained in the exhaust gases which, by expanding in a turbine, provides mechanical work to the shaft of a compressor (turbo-supercharging). The pressure wave supercharger (PWS) also exploits the energy contained in the exhaust gases, but the expansion of gases takes place inside the narrow channels of a rotor containing atmospheric air [22], which is compressed and then sent to the engine intake manifold. PWS uses the phenomenon whereby two fluids placed in direct contact inside narrow channels will equalize their pressures faster than they will mix. It has many advantages, among which: it absorbs minimal power for training and has a good response in transient mode. The main disadvantages are noise, size and lower fuel economy than with turbocharging (for certain speeds).

2.3 THE TECHNOLOGY OF PRESSURE WAVES. SHORT HISTORY

The idea of supercharging appeared more than a century ago, initially applied and tested by Sir Dugald Clark in 1878 on his two-stroke engine, considered to be the first supercharger [20]. In 1885, Gottlieb Daimler patented a technique for forcing air into an internal combustion engine, and in 1896, Rudolf Diesel tested the effect of air pre-compression on the engine performance [15, 21]. Also, in 1902, Louis Renault patented a centrifugal supercharger, almost simultaneously with Sulzer, showing that by increasing the volume of air introduced into the cylinders, more power is produced [22]. The idea of turbocharging was only considered in 1925, when Dr. A. Büchi achieved a 40% increase in power and

demonstrated the advantages of turbocharging [22]. Starting with the year 1938, the company Swiss Machine Work Saurer applied turbocharging to truck engines for the first time. Since then, superchargers have been increasingly applied to serve internal combustion engines, both in commercial vehicles, racing cars and in the naval and aeronautical industries. Their technological complexity and cost limited their widespread use to expensive and high-performance cars until the end of the last century. Today, supercharging is already common place in the automotive industry.

In the middle of the last century, researchers' attention was drawn to a particular type of "compressor", more precisely a pressure exchanger that can increase the air pressure sent to the engine cylinders using, as in the case of turbocharging, the energy of the exhaust gases, with the difference that both fluids are brought into direct contact. It is known as "pressure wave supercharger" (PWS). The processes of gas expansion - air compression take place inside narrow channels along a rotor. The quick response in engine performance for any engine speed makes PWS a good option for supercharging vehicle engines.

The oldest "relative" of the pressure wave compressor was a cell drum called a "semi-static pressure exchanger", patented by Knauff in 1906 [26], followed by a device with a geometry of long and narrow channels proposed by Lebre in 1928 [28]. Approximatively in the same year, Burghard patented [29] a device called a "dynamic pressure exchanger" to distinguish it from Knauff's device. Inside this exchanger, pressure waves are used in both the compression and expansion processes that occur in the rotor channels. In 1940, Claude Seippel of Brown Boveri & Co., trying to apply Lebre's principle to a heat pump, accredited the idea that pressure waves can efficiently transmit energy between two fluids in direct contact [30]. The first wave machine was implemented in Switzerland by Seippel as a high-pressure stage for a gas turbine locomotive engine. Seippel gave the name "COMPREX" to his device, starting from the processes of COMPRession – EXPansion that take place in the rotor channels. The Seipel's rotor had 30 channels and operated at a rotational speed of 6000rpm [30] with an initial pressure ratio of 3:1 and an overall efficiency of 69%, according to tests carried out in 1941-1943 by Brown Boveri & Co. (BBC). The first attempt to implement the new concept of pressure waves in supercharging was made by ITE Circuit Breaker Co. starting in 1949 [15, 30] using Comprex as a supercharger for diesel engines. BBC started PWS development in 1955 [25] and in 1971 the first Comprex® prototype (patented by BBC) was implemented by Valmet Tractors on a truck engine. Around the same year, Mercedes-Benz began testing Comprex for diesel passenger cars [22], followed from 1974 by the car manufacturers Opel, Mazda, Mercedes-Benz, Peugeot and Ferrari. The first success to materialize in limited series production was the Opel Senator model with the 2.3-liter PWS supercharged engine [15], and the first extensive application of Comprex on vehicles was in 1987 on the Mazda 626 Capella equipped with a 2.0-liter engine [31, 32, 35]. The development of Comprex® is due to the work of numerous engineers and researchers who designed, reconfigured and tested its operation in supercharging the engines of many vehicles [35].

A huge step in the implementation of pressure wave devices was achieved by developing soft codes to help solve the equations that describe the processes inside these devices. As such, codes have

been developed for the modeling of non-stationary one-dimensional flow rates, but also the modeling of channel wall friction and heat transfer processes [36] and the modeling of the flow and the main losses, many of which are of two- or three-dimensional nature [37...46].

In the 90s, projects were developed to implement Comprex in various applications: Swissauto WENKO AG started the development of the Swatch-Mobile model, today called Smart, followed by another project developed for GreenPeace called SmILE (Small, Intelligent, Light and Efficient) which had as its main objective the halving of fuel consumption compared to the Renault Twingo series car, while maintaining performance, transport capacity, comfort and safety [15, 52]. The concept was improved over time, and in 2008 the Volkswagen Golf 5 demonstrator was launched with a 1-liter supercharged engine with the new PWS version called Hyprex®, driven by an electric motor and adjusting the boost pressure via a valve in the gas pocket controlled by the ECU [52, 53].

After year 2000, interest in the wave supercharger waned, and the main concern remained with the use of the wave rotor in applications such as wave combustors or in aeronautics. However, some researchers continued to study this particular supercharger. NASA and the Air Force Institute of Technology (AFIT) continued to maintain an interest in pressure wave technology - some of AFIT's thesis approached the subject of pressure wave supercharging on various types of engines serving small or remotely piloted aircraft [54, 55, 56]. Since 2003 the subsidiary ANTROVA AG of 3prex AG Switzerland has registered COMPREX as a trademark and in 2017 obtained the patent for a new improved Comprex [57], thus promoting a new supercharging solution for hydrogen or methane engines as well as a key in keeping the CO2 problem under control [59]. In March 2022, the new PWS, named "Comprex 2.0" revived interest in pressure wave supercharging when, being mounted on a natural gas engine, it proved to be perfectly responsive in all operating conditions. Unlike its turbo counterpart, the engine develops significantly more torque practically from idle, which improves handling and helps save fuel. At the same time, the catalyst heats up six times faster than in a turbo engine, which ensures better values in terms of species in the exhaust gases [60].

In conclusion, it can be stated that, starting with the first pressure exchanger proposed in the 40's up until now, pressure wave technology has established itself as an alternative with proven advantages in the supercharging of internal combustion engines, which deserves increased attention in the current conditions in which it is necessary to increase the performance of already existing engines, using less polluting alternative fuels, or downsizing while preserving the parameters of performance and economy.

2.4 THE PRESSURE WAVE SUPERCHARGER. DESIGN AND CONSTRUCTION.

Over the last century, efforts to improve the performance characteristics and geometry of the wave rotor to suit specific applications have been supported by the continuous progress made in writing codes to solve the equations describing the phenomena specific to PWS operation. The pressure wave supercharger (Fig.3.1) presents significant advantages compared to turbomachines, such as fast

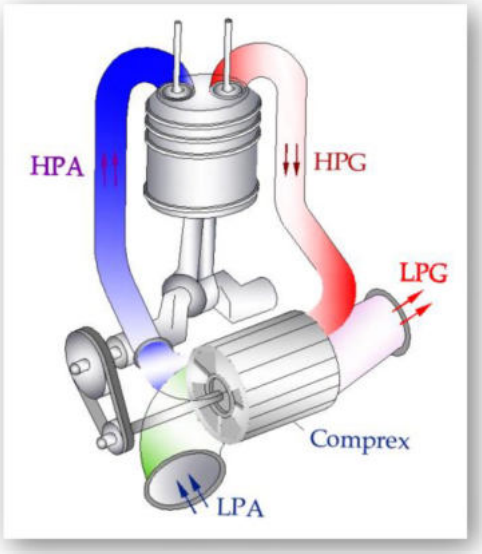

response, simple geometry, minimal channel erosion, low manufacturing costs. However, it raised some challenges, some of a mechanical nature, such as sealing and thermal stress, or of a theoretical nature – the analytical description and solving the equations specific to the phenomena inside the channels [22].

Figure 3.1 – BBC Brown Bovery & Co. Comprex® Pressure wave supercharger.

HPG – high pressure exhaust gases,
HPA – high pressure air,
LPA – low pressure air
GPL – low pressure gases

The PWS operation is based on the transfer of energy from the combustion gases to the intake air by means of shock waves, through short direct contact between the fluids, without using additional mechanical elements; thus, the interaction between hot gases and fresh air induces boost. The device basically consists of a rotor in which narrow longitudinal channels are made, positioned radially on one or two rows (Fig.3.3). The rotor is mounted inside a cylindrical steel casing, having two fixed plates (caps) at the rotor ends, provided with passages that allow the working fluids to flow to or from the manifolds of the engine. The rotor is driven by the crankshaft through a belt or by a separate electric motor [15].

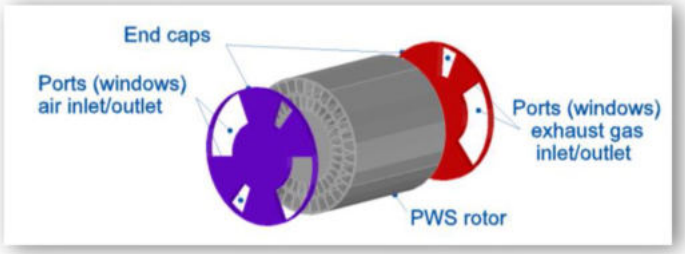

Figure 3.3 – Constructive elements of PWS (simplified presentation)

2.5 PWS OPERATING PRINCIPLES

This can be briefly described by starting from the fact that, as the rotor rotates, the end of its channels are alternately exposed to the intake or exhaust ports, allowing fluids to flow through these „windows". Compression and expansion waves are thus initiated in the rotor channels because of the changes of section when the fluids pass through; the high-pressure gases develop pressure waves that evolve inside the channels and compress the intake charge. The PWS, being a pressure exchanger, overcomes the shortcomings of conventional compressors or turbo-blowers, having the great advantage of changing pressure values in a very short time and therefore tolerating pressure and temperature peaks [15].

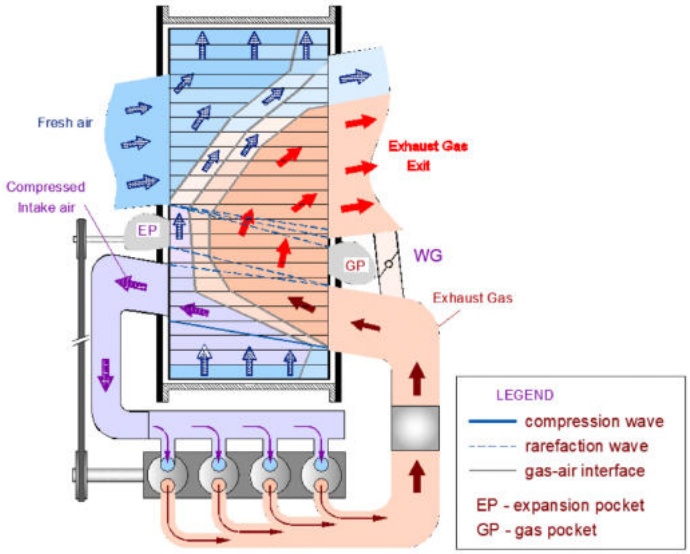

Figure 3.7 – Fluid movement inside the PWS

In Fig.3.7 we have represented the movement of working fluids inside a wave rotor, when operating at an optimal speed. The operation of the Comprex supercharger, viewed from the perspective of pressure wave propagation, was described in detail by Doerfler (1975) of Brown, Bovery & Co. [62]. Fig. 3.8 shows the rotor unfolded in the projection plane and the diagram of the pressure waves. The rotation of the cell drum is translated into a bottom-up movement.

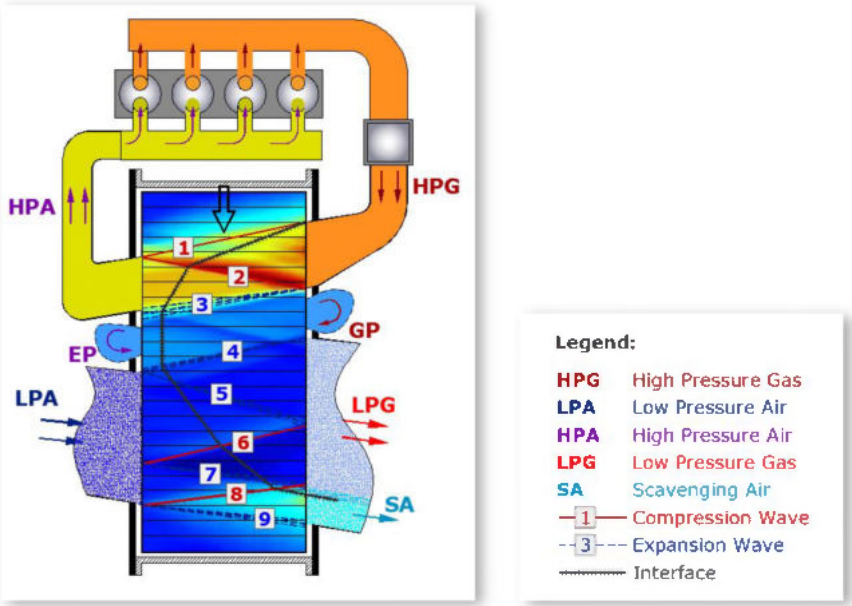

Figure 3.8 - Wave propagation scheme

Noise is one of the shortcomings of the pressure wave supercharger, especially since the conventional Comprex operates over a wide range of speeds, which produces a penetrating type of noise in a frequency band located in the audible zone. The noise level depends mainly on the number of

channels and their sections [72], its reduction being achieved by "breaking" the symmetry of the position of the rotor cells or by using several rows of channels or non-uniform channel sections [22]. In 1985, Prof. Berchtold [65] achieved a noise reduction of about 10 dB by using variable widths of the rotor cells and a difference of 5...15 dB by making rotors with two rows of cells compared to the rotor with a single row of identically sized cells. The maximum noise intensity was approximately 85 dB at 500 Hz, and the minimum was 58 dB recorded at 16 kHz frequencies [65].

The main **advantage** of using pressure waves for ICE supercharging, compared to conventional turbocharging, lies in its direct response to the load, due to the fact that the transfer of the energy of the combustion gases to the intake air is instantaneous [25]. Also, PWS does not present "turbo lag" specific to turbines and is efficient when operating in the entire range of speeds. The light weight and compact configuration of the PWS indicate a potential for use in supercharging small engines (below 75 kW), where turbochargers are in short supply [25]. Other advantages revealed after road testing would be: reduced emissions, better handling with fewer gear changes and reduced sensitivity to imbalances, improved fuel consumption. PWS also has its shortcomings, but nevertheless pressure wave supercharging has reached performance figures that justify further development, confirmed by the new types of Comprex, adjusted for use on "cleaner" engines that use fuels such as natural gas or hydrogen.

CAPITOLUL 3 | MODELING. FLOW EQUATIONS | EXPERIMENTAL RESEARCH IN THE VIRTUAL ENVIRONMENT | RESULTS

3.1 MODELING OF DIMENSIONS AND GEOMETRIC SHAPES

Optimizing the energy and environmental management of the engine in all operating conditions is of particular interest to researchers, but is difficult due to design variables that impose certain specific conditions (operating points) (controllable design parameters) or that are difficult to change (constructive design). Researchers have demonstrated that, through the optimal design of constructive components and the choice of optimal sets of controlled parameters, optimal models can be obtained to facilitate the optimization of the operation of an internal combustion engine [91, 92]. Among the controllable parameters, which can be modified in order to optimize the performance parameters of an ICE, is the intake pressure of the fresh charge. The most common way to increase the power and efficiency of an engine is supercharging. The pressure wave supercharger, as shown in the previous section, has the ability to be dynamically tuned with the engine over its entire range of operating speeds. Thus, the improvement of the design parameters related to the constructive design, with the enhancement of the advantages of the PWS and the reduction of its shortcomings, is a way of optimizing the energy and ecological management of an extended range of ICE by creating additional options for action on the controllable parameters.

The pressure wave supercharger with modified geometry (hereinafter referred to as PWSMG) proposed in this paper, is based on the idea of changing the geometry of the rotor channels so that the fluid flow is improved, the noise is reduced, the degree of supercharging can be increased under the conditions of extending the applicability of this supercharging method to less polluting engines, such as conventional SI or natural gas or hydrogen engines, or to be able to respond to current automotive trends (for example downsizing). The idea of improving the flow is primarily aimed at reducing the pressure losses in the flow of working fluids to/from the rotor channels, aiming to optimize the cross-section of the channels and their shape. The decrease in pressure losses ultimately favors the increase in the degree of supercharging and the performance of the engine in the operating conditions specific to that application. The extension of applicability refers precisely to the possibility of use on engines operating with high speeds or low total cylinder capacity or with high temperatures and pressures of the exhaust gases. Noise reduction is an objective that is achieved by increasing the number of rotor channels and breaking the symmetry of their shape, a method successfully used in existing Comprex models.

The design of the new PWSMG correlated with the real possibilities of experimental research in virtual medium and with those of a theoretical and practical nature, considering the following essential aspects:

- modifying the geometry of the new rotor taking into account the objectives stated above;
- establishing the existing reusable elements in conventional PWS (for example fixed covers), or which can be easily modified, without the application of new technological procedures;
- functionality;
- modeling the new PWSMG, choosing the optimal solution for a general application;
- simulation of operation in the virtual environment;
- the possibility of the implementation of the new PWSMG in practice.

THE PWS CONFIGURATION OPTIMIZATION METHODOLOGY aimed at:

- establishing the shape of the channel section, which will comply with the established objectives and make the practical implementation of the rotor easy;
- establishing the section of the channels, correlated with the increase in the efficiency of use of the surface of the rotor, as well as with the flow rate of the working fluids that cross the said section;
- establishing the number of rows of channels, so that the surface of the port opening is "covered", correlated with the increase of the total surface of the channels simultaneously exposed to the inlet/outlet of the primary fluids, respectively of the secondary ones;
- establishing the channels angle of inclination with respect to the frontal plane of the fixed covers.

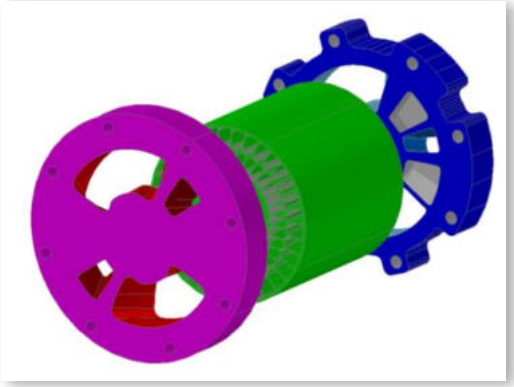

Figura 4.1 – 3-D modeled COMPREX CX–93 supercharger including simplified fixed covers with fluid inlet/outlet ports and gas/compression/expansion pockets and 68-channel rotor

The research was based on the model chosen as a reference, the COMPREX CX–93, the pressure wave supercharger used and consacrated by Mazda on its 626 model, with a 2.0 liter diesel engine. The modeling of each supercharger, both the conventional CX-93 and the new PWSMG, was carried out using an computer aidded design software (AutoCAD) and the model was used for the accuracy of the calculations in the operation simulation (Fig.4.1).

Modeling and analysis of the conventional CX-93 supercharger

A first step in making the geometric changes of the PWS is the analysis of the front surfaces of the passage of the rotor, starting from the geometry and the shape of the conventional supercharger chosen for comparison. The CX-93 modelling was made according to the actual dimensions (Fig. 4.3, 4.4).

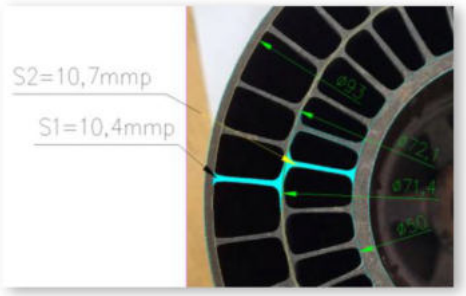

Figure 4.3 – Modeling of the passage surfaces of working fluid at the Comprex CX-93 Rotor

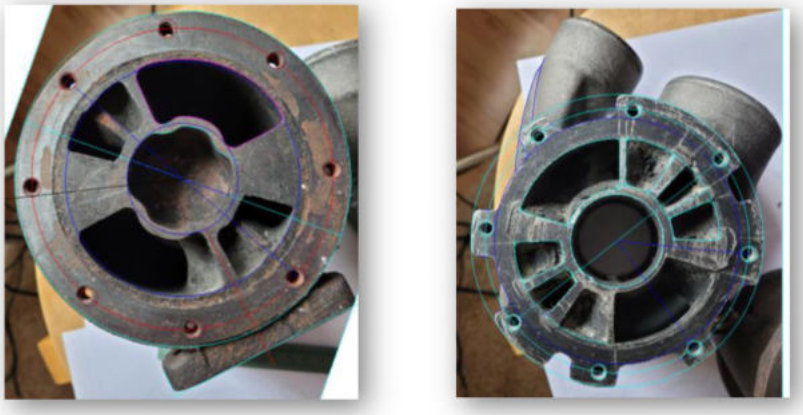

Figure 4.4 – CX-93 fixed covers:
gas passage cover = hot stator (left) and air passage cover = cold stator (right)

b. Establishing the channel section shape of the new PWSMG

The change in the shape of the channel section and modification of the frontal passing surfaces of the rotor are based on optimization calculations and analysis of the dimensions that confer:

1) the largest resulting front surface, by increasing the efficiency of use of the surface;
2) the largest cross-sectional area of the channels, greater than that of CX-93;
3) greater number of channels (CX-93 has 68 channels in total) for noise reduction;
4) shapes of the channel section that improve pressure drops compared to the CX-93;
5) angle of „twisting" of the channels in order to allow an increase of the speed and to take over the supercharging over-pressure.

For modeling of the shape and surfaces of the working fluid passage, a parameter is defined: the surface utilization efficiency, given by the relation:

$$\eta_{uS} = \frac{S_{channel} \cdot N}{\frac{\pi(D_{max}^2 - D_{min}^2)}{4}} \qquad (4.1)$$

where: $S_{channel}$ – the front surface of the channels (the sum of the channel surfaces of the upper, lower or intermediate row);

N – number of channels on a row;

D_{max}, D_{min} – the maximum and minimum diameters of the circles tangent to the upper arc of the outer channel, respectively the lower arc of the inner channel.

For CX-93, the surface utilization efficiency is:

$$\eta_{uS}^{CX} = \frac{118{,}5 \cdot 34}{\frac{\pi(93^2 - 50^2)}{4}} = 0{,}83$$

This is the reference value for further modeling of PWSMG surfaces, for which it is proposed to be increased to a minimum value of 0.87 (5% increase).

Variant 1 – "round" shapes

The investigation of the rotor variant with circular section channels was based on the idea that it improves the flow, considering that it avoids the appearance of turbulence in the "corners" of the trapezoids that represent the section of the PWS Comprex CX-93 channels. The modeling, calculation and choice of the optimal solution were carried out taking into account the maximum and minimum opening diameter of the channels (possible in the CX-93 rotor) and the imposed minimum thickness of the walls of 0.5...0.6mm (Fig. 4.7).

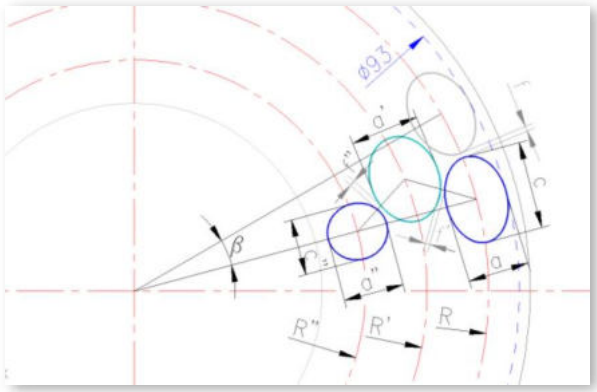

Figure 4.7 – Symbols used for dimensional calculation at PWSMG – variant 1

The calculation elements used in making the model in variant 1 are described below:

f = f' = f'' = min. 0,5 mm

R = 46,5 – a/2 [mm] (4.2)

R' = max (46,5 – a – f – a'/2) [mm] (4.3)

$$R'' = 46{,}5 - a - a' - 2f - a''/2 \qquad [mm] \qquad (4.4)$$

$$N = [n]$$

$$\text{where: } n = \frac{2\cdot\pi\cdot R}{4\cdot R\cdot arcsin\frac{c}{4\cdot R}+f} \qquad (4.5)$$

$$N' = [n'] \quad \text{and} \quad N'' = [n''] \qquad (4.6)$$

$$n' = \frac{2\cdot\pi\cdot R'}{4\cdot R'\cdot arcsin\frac{c}{4\cdot R'}+f'} \quad \text{and} \quad n'' = \frac{2\cdot\pi\cdot R''}{4\cdot R''\cdot arcsin\frac{c}{4\cdot R''}+f''} \qquad (4.7)\ (4.8)$$

The proposed model brought a first variant of the rotor channel shape with circular or elliptical section in the PWS geometry, namely, an optimal solution with 3 rows of channels (Fig. 4.8).

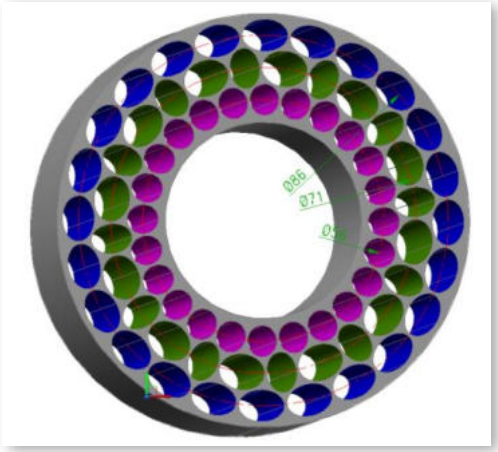

Figure 4.8 – The new rotor of the PWSMG – variant 1

Variant 1 does not fully comply with design condition 2, but the surface values are ± 4 % of the PWS CX-93 surfaces. In addition, the efficiency of use of the surface results:

$$\eta_{uS}^{SUPGM-1} = \frac{(100{,}65 * 24 + 120 * 12)}{\frac{\pi(93^2 - 49^2)}{4}} = 0{,}786$$

reduced from the target value of 0.87. However, the strengths of the variant with elliptical channels consist in the pressure losses comparable to those of the other variants and reduced compared to the CX-93 (as will be shown below), the asymmetry of the arrangement of the channels that predicts reduced noise, increased robustness and easier physical realization of the rotor.

Variant 2 – "trapezoidal" shapes with sloping walls

The investigation of this variant was also carried out respecting the initial design conditions, starting from the shape of the PWS Comprex CX-93 channel section, with the modification of the radial inclination of the channel walls.

The calculation starts from the condition that the surface utilization efficiency is at least 0.87:

$$\eta_{uS}^{SUPGM-2} = \frac{S_{channels} \cdot N}{\frac{\pi(D_{max}^2 - D_{min}^2)}{4}} = min.\,0{,}87 \qquad (4.9)$$

Also, if equation (4.9) is written for the exhaust port, it becomes:

$$\eta_{uS}^{SUPGM-2} = \frac{S_{channels} \cdot N_{HPG}}{S_{HPG}} = min.\,0{,}87 \qquad (4.10)$$

where: N_{HPG} – number of channels exposed in front of the gases port HPG;

S_{HPG} – exhaust gas port surface.

Results:

$$N_{HPG} = \frac{\eta_{uS}^{SUPGM-2} \cdot S_{HPG}}{S_{channels}} \qquad (4.11)$$

Replacing D_{max} = 93mm and D_{min}≈50mm:

$$S_{channels} \cdot N \cong 4200mm^2$$

And for N=36 channels /row (total number of channels per rotor =72):

$$S_{channels} = min.\,116{,}7mm^2$$

The number od channels exposed in front of HPG port:

$$N_{HPG} = \frac{0{,}87 \cdot 269{,}74}{S_{channels}} \approx 2\ chnnels/row$$

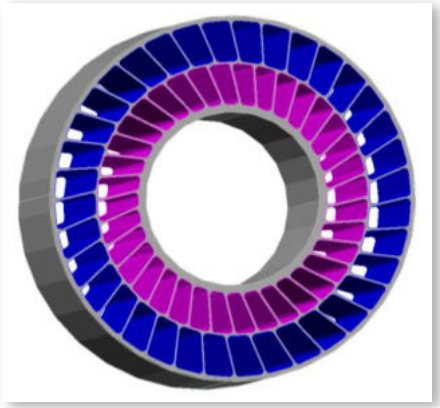

Figure 4.10 – The initial constructive form of the PWSMG – variant 2 overview

Taking into account the dimensions of the HPG port at the maximum diameter and at the minimum diameter, and the minimum wall thickness of 0.6 mm, the preliminary width of the channels (maximum and minimum) is determined. The height of the channels was determined from the condition that it was approximately equal for both rows of channels.

The calculation and choice of the optimal angle of inclination of the channel walls was carried out taking into account previous researches [56...59, 94], but also respecting the previously determined channel widths. It resulted in an inclination of 18° of the walls at a number of 36 cells per row (Fig. 4.10).

It is observed that variant 2 respects the design conditions, with efficiency of using the surface of:

$$\eta_{uS}^{SUPGM-2} = \frac{S_{channels} \cdot N}{\frac{\pi(D_{max}^2 - D_{min}^2)}{4}} = 0{,}871$$

The outer and inner channel rows were offset by an angle of 5° to "break" the symmetry and eliminate the "whistling" noise that characterized Comprex in the early days [27].

Variant 3 – "trapezoidal" shapes with curved walls

The modeling of variant 3 took into account the initial design conditions and was carried out according to the mathematical model used for variant 2. The particularity of this variant consists in the curved shape of the side walls of each channel in the rotor, similar to the way in which the blades of a turbine are curved. A radial inclination of 18° and a unique radius of curvature were determined. The new geometry uses connection radii of 0.5...1.0 mm and wall thickness of min. 0.6mm (Fig. 4.13).

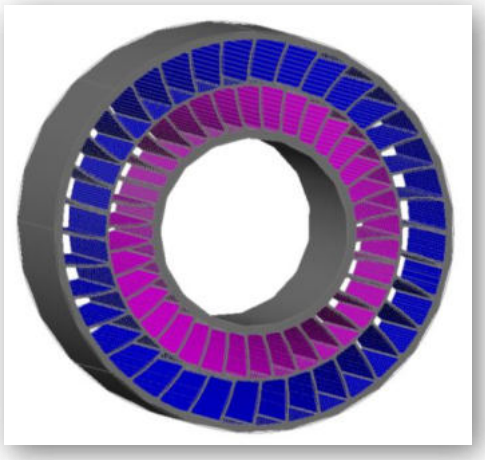

Figure 4.13 – The initial constructive form of the PWSMG – variant 3 overview

Variant 3 of PWSMG complies with the design conditions, having the efficiency of surface use of:

$$\eta_{uS}^{SUPGM-3} = \frac{S_{channels} \cdot N}{\frac{\pi(D_{max}^2 - D_{min}^2)}{4}} = 0{,}875$$

The outer and inner channel rows were offset (rotated) by an angle of 5° to "break" the symmetry and reduce noise [27], but also to increase the exposed front surface of the channels as they gradually open in front of the ports.

3.2 PRESSURE LOSS CALCULATION MODEL

The flow of fluids in channels is accompanied by pressure losses caused by friction and turbulence produced in the areas of section change or flow direction change, losses correlated with the kinetic energy that imprints the movement of the fluid mass and with the potential energy that forms the energy accumulation able to overcome the resistances that oppose the flow. The preliminary validation of variants 1, 2 and 3 of the new PWSMG presupposed the creation of a model for calculating pressure losses when flowing through the rotor channels, under the following calculation assumptions: (i) air and exhaust gases are considered ideal gases; (ii) flow through channels is one-dimensional; (iii) the flow of fresh air discharged directly to the exhaust is zero; (iv) the speed calculation does not take into account the wave phenomena and the peripheral speed of the rotor; (v) channel opening is instantaneous; (vi) no heat exchange takes place.

Thus, frictional pressure losses Δp_R and local pressure losses Δp_ξ can be calculated, which determine the total pressure loss along the fluid flow path [95]:

$$\Delta p = \Delta p_R + \Delta p_\xi \qquad (4.12)$$

where:

- *friction pressure loss is:*

$$\Delta p_R = R \cdot L = \frac{\lambda \cdot \rho \cdot {w_i}^2}{2 \cdot d_e} L \qquad (4.13)$$

R – pressure loss per unit [Pa/m];
L – channel length [m];
λ – coefficient of friction resistance of the inner surface of the channel (dimensionless);
d_e – the equivalent diameter of the channel [m]:

$$d_e = \frac{4 \cdot S}{P} \qquad (4.15)$$

S – cross-sectional area of the canal [m^2];
P – the perimeter "touched" by the fluid [m];
w_i – the average velocity of the fluid in the channel portion "i" considered [m/s];
ρ – fluid density at average temperature, on channel section "i" [kg/m^3];

- *pressure loss due to local resistances:*

$$\Delta p_\xi = \sum_{i=1}^{n} \xi \cdot \frac{\rho \cdot w_i^2}{2} \qquad (4.17)$$

ξ – coefficient of local losses (resistances), which generally depends on the modification of the geometry of the flow paths;
n – the number of channel sections.

The coefficient of friction λ is calculated with the equation for flow in transition zones [95]:

$$\frac{1}{\sqrt{\lambda}} = -2 \cdot \lg\left(\frac{\frac{\varepsilon}{d}}{3{,}71} + \frac{2{,}51}{Re\sqrt{\lambda}}\right) \tag{4.19}$$

Tables 4.1 and 4.2 show the values of the Reynolds number, the ε/de ratio and the iteratively calculated friction coefficient λ, as well as the unit load loss R, necessary for the determination of pressure losses through friction.

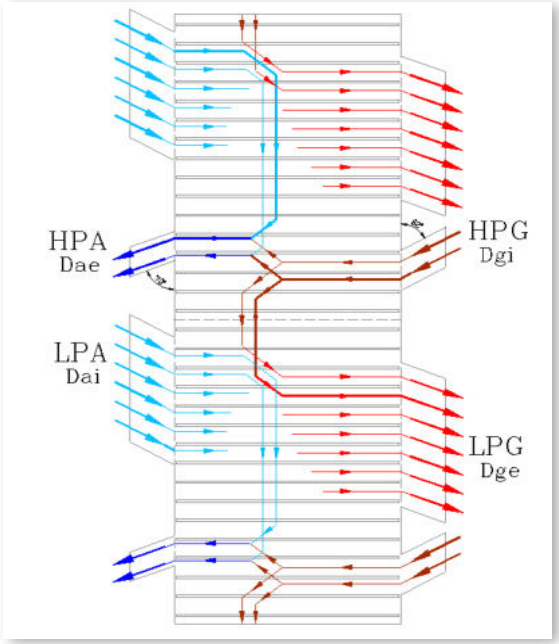

Figure 4.16 – Scheme of gas and air circulation in a rotor represented unfolded, with cells moving from top to bottom

To determine the pressure losses given by the local resistances, the rotor cells (Fig. 4.16) and the flow diagram of the working fluids were represented: the gas circuit - from the HPG port (gas inlet flow Dgi), to the LPG port (gas flow gases coming out of the rotor to the exhaust marked Dge), as well as the air circuit – from the LPA port (air flow entering the rotor Dai) to the HPA port (compressed air flow leaving the rotor to the intake manifold Dae).

The detailed calculation of the pressure losses for the CX-93 and for the three PWSMG variants is presented in Table 4.1 for the variant with straight axial channels and the recirculation of a part of the burnt gases, and in Table 4.2 for the situation where there is no flow of burnt gases to the intake air. The values of the air and gas flows in the four ports are taken from the specialized literature, obtained experimentally, according to [54]. The calculation is a simplified one, its role being to make a comparison between the CX-93 and the PWSMG variants. The flow distribution was calculated under the assumption of maintaining equal velocities on each type of channel. Only channels with close equivalent diameters were considered for comparison. The calculation of pressure losses was carried out considering that both air and gases travel a path of maximum length equal to twice the length of the channels.

In Fig. 4.18 and Fig. 4.19 schematically shows the flow paths of the working fluids and the pressure loss points. Simplified, these points join areas that represent the following types of resistances for the *idealized exhaust gas flow circuit* (Fig. 4.18) and for *the idealized air* circuit inside PWS (Fig.4.19):

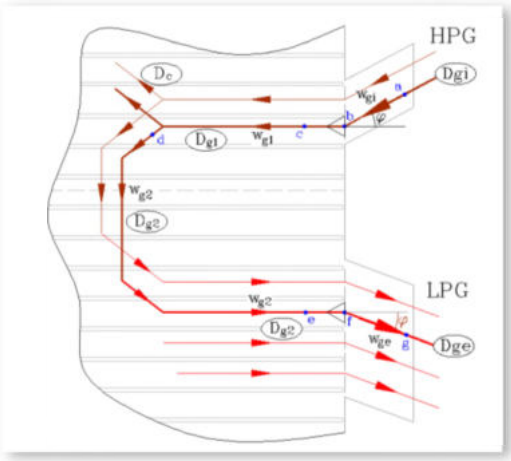

Figure 4.18 – Diagram of pressure loss points on the exhaust gas circuit

- a-b → branch with change of direction at the angle φ (local loss coefficient "csi 1");
- b-c → sudden narrowing of the section (transition from the port section to one channel section);
- c-d › branch with "loss" of flow (reduced speed);
- d-e › "return" of the gases at the left end of the channel (assimilated with two 90° bends);
- e-f › steep widening of the section (transition from a channel section to the section of the port);
- f-g › branch with change of direction at angle φ.

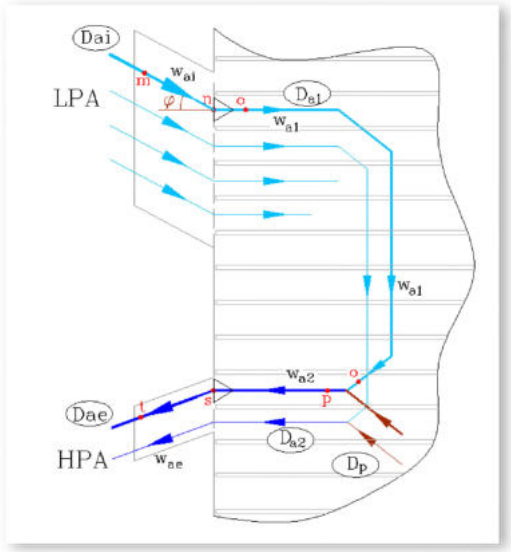

Figure 4.19 – Diagram of pressure loss points on the air circuit

- m-n → branch with change of direction at the angle φ;
- n-o → sudden narrowing of the section (transition from the section of the port to the section of a channel);

- o-p → "return" of the gases at the left end of the channel (assimilated with two 90° bends);
- p-s → steep section widening (transition from channel section to outlet port section)
- s-t → branch with change of direction at angle φ.

From the calculation summarized in Table 4.1, it can be seen that on the gas "route" the pressure loss in CX-93 and PWSMG - variants 1, 2 and 3 is ~0.31 bar, the differences compared to CX-93 being small, in favor of PWSMG. On the air path, the CX-93 is seen to have an estimated loss of 0.146 bar, while versions 1 and 2 of the PWSMG show 0.13 bar and version 3 a 0.122 bar, 16.5% less than the CX-93.

In Table 4.2 the ideal case "without EGR" was calculated, noting that the variants considered for the new PWSMG present pressure losses on the gas path approximately equal to 0.34...0.35 bar, lower compared to CX-93 which registers a pressure loss of 0.37 bar, and in the air path, the PWSMG variants have pressure losses of 0.084...0.096 bar, while Comprex presents losses of 0.10 bar, with 4...19 % higher compared to the new PWSMG.

It should be noted that the pressure loss values are calculated under the conditions of keeping the dimensions of the ports practiced in the end caps, as well as the length of the rotor of 93mm. According to the obtained values, it can be concluded that:

- PWSMG - variant 1, for which the front surface is 94% of that of the CX-93, presents pressure losses comparable to the CX-93, the explanation being found in the fact that the "round" shapes induce lower pressure losses compared to the shapes "trapezoidal" where the flow in the "corner" sections is strongly turbulent;
- PWSMG – variant 3, respectively variant 2 presents the lowest pressure losses compared to CX-93 and variant 1, the differences between variants 2 and 3 can be considered negligible.

Table 4.1. Calculation of pressure losses in the channels of the Comprex CX-93 pressure wave SUPERcharger, respectively PWSMG – variants 1, 2 and 3 – without axial inclination angle of the channels

beta	Supraf.trecere in capac		Supraf.canale expuse		Supraf.	P	Diam.echiv.	Debit intrare	Debit iesire	Debit/canal	Viteza in capac	Viteza in capac	Vit.intrare in	Vit.compusa	Debit primit/	Vit.2 in canal	Coef.pierderi locale (cs				Coef.pierd.longit.		Lung. max	Δp
	CX-93 traseu gaze evacuare				canal tip x	perim.canal	[mm]	[m3/h]	[m3/h]	[m3/h]	intrare [m/s]	iesire [m/s]	canal x [m/s]		cedat	x [m/s]	csi 1	csi 2	csi 3	csi 4	R1 [Pa/m]	R2 [Pa/m]	canal [m]	[bar]
	S(HPG)c	S(LPG)c	S(HPG)	S(LPG)	S(x)		de	Dgi	Dge	Dg1	wgi	wge	wg1		cedat	wg2								
	264,9	1240,07	224,4	957,2	69,2	31,98	**8,66**	360	300	55,51	188,75	33,60	**222,82**	**194,88**	9,25	**185,68**	0,40	0,36	1,80	0,8	62306,53	56563,01	0,186	**0,310666**
	264,9	1240,07	224,4	957,2	49,2	28,1	7,00	360	300	39,47	188,75	33,60	222,82	194,88	6,58	185,68							0,186	
	CX-93 traseu aer																							
	S(LPA)c	S(HPA)c	S(LPA)	S(HPA)	S(x)		de	Dai	Dae	Da1	wai	wae	wa1		primit	wa2								
0	1034	227,55	802,6	178,4	69,2	31,88	**8,68**	240	300	10,35	32,24	183,11	**41,53**	**36,32**	2,59	**51,91**	0,70	3,12	1,40	1,44	6564,984	13595,82	0,186	**0,14672**
0	1034	227,55	802,6	178,4	49,2	28,1	7,00	240	300	7,36	32,24	183,11	41,53	36,32	1,84	51,91							0,186	
	SUPGM varianta 1		traseu gaze evacuare																					
	S(HPG)c	S(LPG)c	S(HPG)	S(LPG)	S(x)		de	Dgi	Dge	Dg1	wgi	wge	wg1		cedat	wg2								
0	264,9	1240,07	217,9	922,3	39,00	22,2	7,03	360	300	32,22	188,75	33,60	229,46	**200,69**	5,37	191,22							0,186	
0	264,9	1240,07	217,9	922,3	68,72	29,7	9,26	360	300	56,77	188,75	33,60	229,46	200,69	9,46	191,22							0,186	
0	264,9	1240,07	217,9	922,3	51,27	25,8	7,95	360	300	42,35	188,75	33,60	229,46	200,69	7,06	191,22							0,186	
0	264,9	1240,07	217,9	922,3	61,66	28,51	**8,65**	360	300	50,94	188,75	33,60	**229,46**	200,69	8,49	191,22	0,40	0,26	1,80	0,8	62388,22	59173,16	0,186	**0,311106**
	SUPGM varianta 1		traseu aer																					
	S(LPA)c	S(HPA)c	S(LPA)	S(HPA)	S(x)		de	Dai	Dae	Da1	wai	wae	wa1		primit	wa2								
0	1034	227,55	787,9	184,4	39,00	22,93	6,80	240	300	5,94	32,24	183,11	**42,31**	37,00	1,48	**52,88**							0,186	
0	1034	227,55	787,9	184,4	68,72	29,46	9,33	240	300	10,47	32,24	183,11	42,31	37,00	2,62	52,88							0,186	
0	1034	227,55	787,9	184,4	51,27	25,61	8,01	240	300	7,81	32,24	183,11	42,31	37,00	1,95	52,88							0,186	
0	1034	227,55	787,9	184,4	61,66	28,3	**8,72**	240	300	9,39	32,24	183,11	42,31	37,00	2,35	52,88	0,70	3,12	1,40	1,25	6692,468	13997,29	0,186	**0,13522**
	SUPGM varianta 2		traseu gaze evacuare																					
	S(HPG)c	S(LPG)c	S(HPG)	S(LPG)	S(x)		de	Dgi	Dge	Dg1	wgi	wge	wg1		cedat	wg2								
0	264,9	1240,07	231,4	1002,9	69,39	34,1	**8,14**	360	300	53,98	188,75	33,60	**216,08**	**188,98**	9,00	**180,06**	0,40	0,26	1,80	0,8	64150	58156,89	0,186	**0,306332**
0	264,9	1240,07	231,4	1002,9	48,39	30,8	6,28	360	300	37,64	188,75	33,60	216,08	188,98	6,27	180,06							0,186	
	SUPGM varianta 2		traseu aer																					
	S(LPA)c	S(HPA)c	S(LPA)	S(HPA)	S(x)		de	Dai	Dae	Da1	wai	wae	wa1		primit	wa2								
0	1034	227,55	844,1	202,5	69,39	34,1	**8,14**	240	300	9,86	32,24	183,11	**39,49**	**34,54**	2,47	**49,36**	0,70	3,30	1,40	1,3	6419,184	13183,62	0,186	**0,135653**
0	1034	227,55	844,1	202,5	48,39	30,8	6,28	240	300	6,88	32,24	183,11	39,49	34,54	1,72	49,36							0,186	
	SUPGM varianta 3		traseu gaze evacuare																					
	S(HPG)c	S(LPG)c	S(HPG)	S(LPG)	S(x)		de	Dgi	Dge	Dg1	wgi	wge	wg1		cedat	wg2								
0	264,9	1248	231,9	1009,8	69,48	33,9	**8,20**	360	300	53,93	188,75	33,39	**215,61**	**188,58**	8,99	**179,68**	0,40	0,24	1,80	0,8	63156,54	57492,18	0,186	**0,30158**
0	264,9	1248	231,9	1009,8	48,84	29,8	6,56	360	300	37,91	188,75	33,39	215,61	188,58	6,32	179,68							0,186	
	SUPGM varianta 3		traseu aer																					
	S(LPA)c	S(HPA)c	S(LPA)	S(HPA)	S(x)		de	Dai	Dae	Da1	wai	wae	wa1		primit	wa2								
0	1040	240,6	850	201,4	69,48	33,9	**8,20**	240	300	9,81	32,05	173,18	**39,22**	**34,30**	2,45	**49,02**	0,70	3,30	1,40	1,25	6259,27	12925,82	0,186	**0,122404**
0	1040	240,6	850	201,4	48,84	29,8	6,56	240	300	6,90	32,05	173,18	39,22	34,30	1,72	49,02							0,186	

	Reynolds	Epsilon/d	Lambda	R [Pa/m]
CX-93				
wg1	37483,6197	0,04621387	0,071	62306,5263
wg2	35714,2076	0,04621387	0,071	56563,0122
wa1	21025,9372	0,04606936	0,072	6564,98399
wa2	19597,9001	0,04621387	0,073	13595,8243
SUPGM-1				
wg1	38582,0957	0,04623743	0,067	62388,2164
wg2	36760,83	0,04623743	0,07	59173,1648
wa1	21498,7258	0,04589685	0,071	6692,46841
wa2	20038,5779	0,04589685	0,0727	13997,2881

	Reynolds	Epsilon/d	Lambda	R [Pa/m]
SUPGM-2				
wg1	34183,45018	0,049142528	0,0731	64150,00429
wg2	32569,82235	0,049142528	0,073	58156,88855
wa1	18741,97458	0,049142528	0,073	6419,183907
wa2	17469,05941	0,049142528	0,0734	13183,61544
SUPGM-2				
wg1	34355,48656	0,048791019	0,0728	63156,53587
wg2	32733,73776	0,048791019	0,073	57492,17941
wa1	18745,97019	0,048791019	0,0727	6259,270422
wa2	17472,78365	0,048791019	0,0735	12925,82143

Table 4.2. – Calculation of pressure losses in the SUPacharger channels with Comprex CX-93 pressure waves, respectively PWSMG – variants 1, 2 and 3 – without gas penetration into the intake air (without EGR effect)

beta	Supraf.trecere in capac		Supraf.canale expuse		Supraf.	P	Diam.echiv.	Debit intrare	Debit iesire	Debit/canal	Viteza in capac	Viteza in capac	Vit.intrare in	Vit.	Debit primit/	Vit.2 in canal	Coef.pierderi locale (cs				Coef.pierd.longit.		Lung. max	Δp
	CX-93 traseu gaze evacuare				canal tip x	perim.canal	[mm]	[m3/h]	[m3/h]	[m3/h]	intrare [m/s]	iesire [m/s]	canal x [m/s]	compusa	cedat	x [m/s]	csi 1	csi 2	csi 3	csi 4	R1 [Pa/m]	R2 [Pa/m]	canal [m]	[bar]
	S(HPG)c	S(LPG)c	S(HPG)	S(LPG)	S(x)		de	Dgi	Dge	Dg1	wgi	wge	wg1		cedat	wg2								
	264,9	1240,07	224,4	957,2	69,2	31,88	**8,68**	360	360	55,51	188,75	40,32	**222,82**	**194,88**	0,00	**222,82**	0,40	0,36	1,80	0,8	62111,7	81196,04	0,186	**0,37071**
	264,9	1240,07	224,4	957,2	49,2	28,01	7,03	360	360	39,47	188,75	40,32	222,82	194,88	0,00	222,82							0,186	
	CX-93 traseu aer																							
	S(LPA)c	S(HPA)c	S(LPA)	S(HPA)	S(x)		de	Dai	Dae	Da1	wai	wae	wa1		primit	wa2								
0	1034	227,55	802,6	178,4	69,2	31,88	**8,68**	240	240	10,35	32,24	146,49	**41,53**	**36,32**	0,00	**41,53**	0,70	3,12	1,40	1,44	6564,984	8939,72	0,186	**0,10226**
0	1034	227,55	802,6	178,4	49,2	28,01	7,03	240	240	7,36	32,24	146,49	41,53	36,32	0,00	41,53							0,186	
	SUPGM varianta 1		traseu gaze evacuare																					
	S(HPG)c	S(LPG)c	S(HPG)	S(LPG)	S(x)		de	Dgi	Dge	Dg1	wgi	wge	wg1		cedat	wg2								
0	264,9	1240,07	217,9	922,3	39,00	22,93	6,80	360	360	32,22	188,75	40,32	229,46	**200,69**	0,00	229,46							0,186	
0	264,9	1240,07	217,9	922,3	68,72	29,46	9,33	360	360	56,77	188,75	40,32	229,46	200,69	0,00	229,46							0,186	
0	264,9	1240,07	217,9	922,3	51,27	25,61	8,01	360	360	42,35	188,75	40,32	229,46	200,69	0,00	229,46							0,186	
0	264,9	1240,07	217,9	922,3	61,66	28,3	**8,72**	360	360	50,94	188,75	40,32	**229,46**	200,69	0,00	229,46	0,40	0,26	1,80	0,8	61928,67	72498,62	0,186	**0,35046**
	SUPGM varianta 1		traseu aer																					
	S(LPA)c	S(HPA)c	S(LPA)	S(HPA)	S(x)		de	Dai	Dae	Da1	wai	wae	wa1		primit	wa2								
0	1034	227,55	787,9	184,4	39,00	22,93	6,80	240	240	5,94	32,24	146,49	**42,31**	37,00	0,00	**42,31**							0,186	
0	1034	227,55	787,9	184,4	68,72	29,46	9,33	240	240	10,47	32,24	146,49	42,31	37,00	0,00	42,31							0,186	
0	1034	227,55	787,9	184,4	51,27	25,61	8,01	240	240	7,81	32,24	146,49	42,31	37,00	0,00	42,31							0,186	
0	1034	227,55	787,9	184,4	61,66	28,3	**8,72**	240	240	9,39	32,24	146,49	42,31	37,00	0,00	42,31	0,70	3,12	1,40	1,25	6692,468	9118,453	0,186	**0,09496**
	SUPGM varianta 2		traseu gaze evacuare																					
	S(HPG)c	S(LPG)c	S(HPG)	S(LPG)	S(x)		de	Dgi	Dge	Dg1	wgi	wge	wg1		cedat	wg2								
0	264,9	1240,07	231,4	1002,9	69,39	33,93	**8,18**	360	360	53,98	188,75	40,32	**216,08**	**188,98**	0,00	**216,08**	0,40	0,26	1,80	0,8	63830,19	76479,51	0,186	**0,35359**
0	264,9	1240,07	231,4	1002,9	48,39	30,66	6,31	360	360	37,64	188,75	40,32	216,08	188,98	0,00	216,08							0,186	
	SUPGM varianta 2		traseu aer																					
	S(LPA)c	S(HPA)c	S(LPA)	S(HPA)	S(x)		de	Dai	Dae	Da1	wai	wae	wa1		primit	wa2								
0	1034	227,55	844,1	202,5	69,39	33,93	**8,18**	240	240	9,86	32,24	146,49	**39,49**	**34,54**	0,00	**39,49**	0,70	3,30	1,40	1,3	6387,182	8692,837	0,186	**0,09492**
0	1034	227,55	844,1	202,5	48,39	30,66	6,31	240	240	6,88	32,24	146,49	39,49	34,54	0,00	39,49							0,186	
	SUPGM varianta 3		traseu gaze evacuare																					
	S(HPG)c	S(LPG)c	S(HPG)	S(LPG)	S(x)		de	Dgi	Dge	Dg1	wgi	wge	wg1		cedat	wg2								
0	264,9	1248	231,9	1009,8	69,48	33,5	**8,30**	360	360	53,93	188,75	40,06	**215,61**	**188,58**	0,00	**215,61**	0,40	0,24	1,80	0,8	62411,33	75087,62	0,186	**0,34663**
0	264,9	1248	231,9	1009,8	48,84	29,45	6,63	360	360	37,91	188,75	40,06	215,61	188,58	0,00	215,61							0,186	
	SUPGM varianta 3		traseu aer																					
	S(LPA)c	S(HPA)c	S(LPA)	S(HPA)	S(x)		de	Dai	Dae	Da1	wai	wae	wa1		primit	wa2								
0	1040	240,6	850	201,4	69,48	33,5	**8,30**	240	240	9,81	32,05	138,54	**39,22**	**34,30**	0,00	**39,22**	0,70	3,30	1,40	1,25	6185,415	8452,973	0,186	**0,08607**
0	1040	240,6	850	201,4	48,84	29,45	6,63	240	240	6,90	32,05	138,54	39,22	34,30	0,00	39,22							0,186	

	Reynolds	Epsilon/d	Lambda	R [Pa/m]
CX-93				
wg1	37601,197	0,04606936	0,071	62111,697
wg2	42991,481	0,04606936	0,071	81196,045
wa1	21025,937	0,04606936	0,072	6564,984
wa2	15678,32	0,04606936	0,075	8939,7201
SUPGM-1				
wg1	38868,394	0,04589685	0,067	61928,675
wg2	44440,336	0,04589685	0,06	72498,616
wa1	21498,726	0,04589685	0,071	6692,4684
wa2	16030,862	0,04589685	0,074	9118,4534

	Reynolds	Epsilon/d	Lambda	R [Pa/m]
SUPGM-2				
wg1	34354,72005	0,0489	0,0731	63830,19488
wg2	39279,60892	0,0489	0,067	76479,5068
wa1	18835,87778	0,0489	0,073	6387,18211
wa2	14045,26793	0,0489	0,076	8692,836546
SUPGM-2				
wg1	34765,70132	0,04822	0,0728	62411,32601
wg2	39749,50603	0,04822	0,067	75087,61597
wa1	18969,80267	0,04822	0,0727	6185,414724
wa2	14145,13112	0,04822	0,076	8452,973116

3.3 CALCULATION OF THE INCLINATION ANGLE OF CHANNELS

One of the objectives of the present research is to modify the geometry of the rotor so that it can be used in the supercharging of an extended range of engines, other than diesel ones, for example SI, natural gas or hydrogen engines. Most of these engines that equip the current vehicle fleet are characterized by rated operating speeds higher than compression ignition engines, which would, in the case of PW supercharging, increase the rotor speed and affect the optimum operating values of the pressure wave supercharger. To ensure the optimum operation of the PWS on a range of engines with higher rated speeds or higher intake air requirements than the engine considered as the basis of comparison and analysis - the Mazda 626 2.0 liter engine for which it was designed and improved the Comprex CX-93 supercharger - it was proposed in this work to use the new PWSMG optimised by the modification of the axial direction of channels. This is realized by inclining the channel direction according to a helical direction with a certain angle relative to the longitudinal generator.

The technical data of Mazda 2.0 liter diesel engine is shown in Table 4.3:

Table 4.3. Technical characteristics of the diesel engine that equips the Mazda 626 model

Parameter	Value
Effective power / rated speed	60,3 kW at 4000 rpm
Torque/ speed	161 Nm at 2000 rpm
Displacement	2 liter
No. Of cylinders	4 in line
Bore	86 mm
Stroke	86 mm
Compression ratio	21,1:1
Consumption	6,8 liter/100km

For extended application of the new PWSMG to engines of higher speeds and/or low displacement, a symbolic engine named M-6000 supcharged with PWSMG will be considered for simplification and generalization, which will be used in the comparative investigation with the engine Mazda 626. The research will consider, as practiced in PWS related research, operating parameters established for the M-6000 engine [34, 47, 48, 54, 56, 64, 96, etc.].

The air flow required for combustion for a 4-stroke engine can be calculated according to the engine speed n, the displacement V_H and the volumetric efficiency η_v (considered equal to unity for simplification). Also, the flow rate of combustion gases can be considered equal to the air flow, if the fuel flow is neglected.

$$\dot{m}_a = \rho_a V_H \cdot \frac{n_{motor}}{30 \cdot \tau} \cdot \eta_v = \frac{p_A}{R \cdot T_A} \cdot V_H \cdot \frac{n_{motor}}{30 \cdot \tau} \cdot \eta_v \qquad (4.23)$$

It can thus be stated that the air mass flow rate depends on the product between the cylinder capacity and the engine speed. In order to preserve the general character in the applications of the new

PWSMG, a *ratio* was calculated between the product of *cylinder capacity x engine speed and the same product corresponding to the Mazda 626* reference engine (Table 4.5), for which the literature provides research data from recent years. It is observed that this ratio varies between 1.0...1.5, so, for example, for M-6000 engine speed ≈50% higher than the nominal speed of the reference engine, the mass air flow required by M-6000 will be maximum 50% higher than the required flow for which the Comprex CX-93 was designed, keeping constant the values of the other parameters involved (volumetric efficiency, pressure and temperature of the intake air).

Table 4.5. Comparison of rpm x displacement ratio for different engine types, relative to Mazda 626 engine ratio

Fuel	Model	Displacement V_H [l]	Power [kW]	Speed n [rot/min]	n x V_H /2x4000
gasoline	Toyota Corolla	1,6	98	6400	1,3
gasoline	Golf 5	1,6	75	5600	1,12
gasoline	Mazda3 1.4 s-vt	1,35	62,6	6000	1,01
gasoline [103]	Ford Duratec	2,3	107	5250	1,50
gasoline	Mercedes 270 DE16	1,6	75	6000	1,2
gasoline	Renault k-Type	1,6	72	5750	1,15
hydrogen [103]	Ford Duratec	2,3	55	4000	1,15
hydrogen [104]	DCC/VM Motori	2,5	103	4000	1,25
CNG	[105]	1,6	110	6000	1,2

The working principle of the PWS is primarily based on the primary wave generated by the entry of the exhaust gases from the exhaust manifold into the rotor channels, so the state parameters of the exhaust gases have a significant importance in the performance of the PWS. It can be considered that the exhaust gas flow rate is equal to the required air flow rate, and the exhaust gas temperature ratio, at the same exhaust gas pressure, is:

$$T_{g-M6000} \approx 1{,}2 \cdot T_{g-Mazda}$$

It results in a velocity ratio in the HPG port for an identical flow surface of:

$$V_g^{MGPWS} \approx 1{,}6\, V_g^{CX}$$

To choose the angle of inclination, the composition equations of the speed vectors were wrotten for the PWSMG (Fig. 4.21), in which V_T is the peripheral speed of the PWSMG rotor, Vg the gas speed in the HPG port, Wg the fluid speed relative to the rotor [102]. It is deduced that:

$$V_T = 1{,}6 \cdot V_g^{CX}(sin\varphi - cos\varphi \cdot tg\beta)$$

resulting: $\beta = 8°\ and\ L \approx 58\ mm$ (new rotor length).

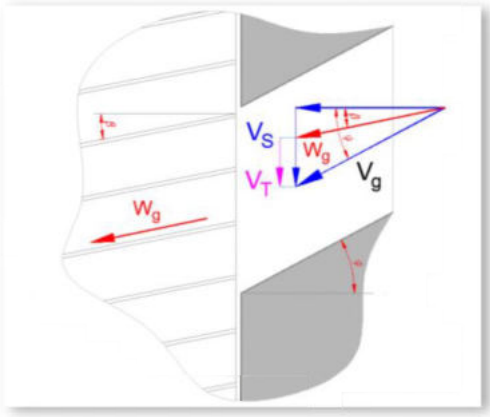

Figure 4.21 – Velocity vectors in PWSMG

Fig. 4.23 shows the unfolded image of the rotor. The new configuration causes the reduction of the cross section of the channel, so the pressure losses increase in the new configuration compared to the preliminary calculations. In Table 4.6, the pressure loss calculation of the PWSMG is presented, under the same assumptions as those in the preliminary calculation, for comparison. It is observed that, for the PWSMG, the pressure drops are lower by 30...40% compared to the CX-93.

Table 4.7 presents the calculations for the CX-93 and for the 3 PWSMG variants, imposing air flow rates increased by 50% compared to the preliminary calculation, limit flow rates for the symbolic M-6000 engine. It can be observed that pressure loss in the air path is 50% lower compared to CX-93, which confirms that the new configuration ensures operation at increased flow rates. It should be noted that version 3 of PWSMG is the most advantageous, this variant being further researched in the virtual media.

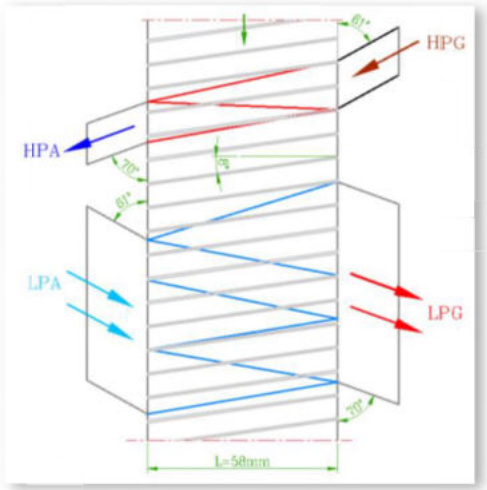

Figure 4.23 –Unfolded rotor relative to the circumference of the average diameter of the outer row of channels

Table 4.6 Calculation of pressure losses in the channels of PWSMG – variants 1, 2 and 3 – with the axial inclination angle of the channels and flow rates identical to the preliminary calculation

beta	Supraf.trecere in capac		Supraf.canale expuse		Supraf.	P	Diam.echiv.	Debit intrare	Debit iesire	Debit/canal	Viteza in capac	Viteza in capac	Vit.intrare in	Viteza	Debit primit/	Vit.2 in canal	Coef.pierderi locale (csi)				Coef.pierd.longit.		Lung. max	Δp
					canal tip x	perim.canal	[mm]	[m3/h]	[m3/h]	[m3/h]	intrare [m/s]	iesire [m/s]	canal x [m/s]	compusa	cedat	x [m/s]	csi 1	csi 2	csi 3	csi 4	R1 [Pa/m]	R2 [Pa/m]	canal [m]	[bar]
	SUPGM varianta 1		traseu gaze evacuare																				2*L/cos(b)	
	S(HPG)c	S(LPG)c	S(HPG)	S(LPG)	S(x)		de	Dgi	Dge	Dg1	wgi	wge	wg1		cedat	wg2								
8	264,9	1240,07	217,9	922,3	38,62	22,93	6,74	360	300	31,90	188,75	33,60	229,46	**202,67**	5,32	191,22							0,11714	
8	264,9	1240,07	217,9	922,3	68,05	29,46	9,24	360	300	56,21	188,75	33,60	229,46	202,67	9,37	191,22							0,11714	
8	264,9	1240,07	217,9	922,3	50,77	25,61	7,93	360	300	41,94	188,75	33,60	229,46	202,67	6,99	191,22							0,11714	
8	264,9	1240,07	217,9	922,3	61,06	28,3	**8,63**	360	300	50,44	188,75	33,60	**229,46**	202,67	8,41	191,22	0,04	0,26	1,40	0,8	67579,82	60161,9	0,11714	**0,201763**
	SUPGM varianta 1		traseu aer																					
	S(LPA)c	S(HPA)c	S(LPA)	S(HPA)	S(x)		de	Dai	Dae	Da1	wai	wae	wa1		primit	wa2								
8	1034	227,55	787,9	184,4	38,62	22,93	6,74	240	300	5,88	32,24	183,11	**42,31**	37,37	1,47	**52,88**							0,11714	
8	1034	227,55	787,9	184,4	68,05	29,46	9,24	240	300	10,36	32,24	183,11	42,31	37,37	2,59	52,88							0,11714	
8	1034	227,55	787,9	184,4	50,77	25,61	7,93	240	300	7,73	32,24	183,11	42,31	37,37	1,93	52,88							0,11714	
8	1034	227,55	787,9	184,4	61,06	28,3	**8,63**	240	300	9,30	32,24	183,11	42,31	37,37	2,32	52,88	0,10	3,12	1,40	1,25	6988,793	14193,18	0,11714	**0,12046**
	SUPGM varianta 2		traseu gaze evacuare																					
	S(HPG)c	S(LPG)c	S(HPG)	S(LPG)	S(x)		de	Dgi	Dge	Dg1	wgi	wge	wg1		cedat	wg2								
8	264,9	1240,07	231,4	1002,9	68,71	33,93	**8,10**	360	300	53,45	188,75	33,60	**216,08**	**190,84**	8,91	**180,06**	0,04	0,26	1,40	0,8	65640,72	58435,65	0,11714	**0,192097**
8	264,9	1240,07	231,4	1002,9	47,92	30,66	6,25	360	300	37,27	188,75	33,60	216,08	190,84	6,21	180,06							0,11714	
	SUPGM varianta 2		traseu aer																					
	S(LPA)c	S(HPA)c	S(LPA)	S(HPA)	S(x)		de	Dai	Dae	Da1	wai	wae	wa1		primit	wa2								
8	1034	227,55	844,1	202,5	68,71	33,93	**8,10**	240	300	9,77	32,24	183,11	**39,49**	**34,88**	2,44	**49,36**	0,10	3,30	1,40	1,3	6577,35	13264,86	0,11714	**0,121333**
8	1034	227,55	844,1	202,5	47,92	30,66	6,25	240	300	6,81	32,24	183,11	39,49	34,88	1,70	49,36							0,11714	
	SUPGM varianta 3		traseu gaze evacuare																					
	S(HPG)c	S(LPG)c	S(HPG)	S(LPG)	S(x)		de	Dgi	Dge	Dg1	wgi	wge	wg1		cedat	wg2								
8	269,74	1253,1	231,9	1009,8	68,80	33,5	**8,22**	360	300	53,41	185,36	33,25	**215,61**	**190,43**	8,90	**179,68**	0,04	0,24	1,40	0,8	64446,09	57372,15	0,11714	**0,187666**
8	269,74	1253,1	231,9	1009,8	48,36	29,45	6,57	360	300	37,54	185,36	33,25	215,61	190,43	6,26	179,68							0,11714	
	SUPGM varianta 3		traseu aer																					
	S(LPA)c	S(HPA)c	S(LPA)	S(HPA)	S(x)		de	Dai	Dae	Da1	wai	wae	wa1		primit	wa2								
8	1040	240,6	850	201,4	68,80	33,5	**8,22**	240	300	9,71	32,05	173,18	**39,22**	**34,64**	2,43	**49,02**	0,10	3,30	1,40	1,25	6395,86	12898,83	0,11714	**0,108231**
8	1040	240,6	850	201,4	48,36	29,45	6,57	240	300	6,83	32,05	173,18	39,22	34,64	1,71	49,02							0,11714	

	Reynolds	Epsilon/d	Lambda	R [Pa/m]
SUPGM-1				
wg1	38868,3939	0,04634791	0,071	67579,8164
wg2	36673,205	0,04634791	0,071	60161,9007
wa1	21498,7258	0,04634791	0,072	6988,79258
wa2	19843,5639	0,04634791	0,073	14193,1756
SUPGM-2				
wg1	34354,72	0,04937808	0,073	65640,7187
wg2	32414,4521	0,04937808	0,073	58435,6486
wa1	18835,8778	0,04937808	0,073	6577,3503
wa2	17385,7254	0,04937808	0,0735	13264,8551
SUPGM-3				
wg1	34765,7013	0,04868915	0,073	64446,0886
wg2	32802,2221	0,04868915	0,073	57372,1474
wa1	18969,8027	0,04868915	0,073	6395,85997
wa2	17509,3396	0,04868915	0,0735	12898,8349

Table 4.7 Calculation of pressure losses in the channels of CX-93 and PWSMG - variants 1, 2 and 3 - with axial inclination angle of the channels and air flows 50% higher than in the preliminary calculation, assuming the operation on the M6000 engine

beta	Supraf.trecere in capac		Supraf.canale expuse		Supraf.	P	Diam.echiv.	Debit intrare	Debit iesire	Debit/canal	Viteza in capac	Viteza in capac	Vit.intrare in	Vit.	Debit primit/	Vit.2 in canal	Coef.pierderi locale (cs				Coef.pierd.longit.		Lung. max	Δp
0	CX-93	traseu gaze evacuare			canal tip x	perim.canal	[mm]	[m3/h]	[m3/h]	[m3/h]	intrare [m/s]	iesire [m/s]	canal x [m/s]	compusa	cedat	x [m/s]	csi 1	csi 2	csi 3	csi 4	R1 [Pa/m]	R2 [Pa/m]	canal [m]	[bar]
0	S(HPG)c	S(LPG)c	S(HPG)	S(LPG)	S(x)		de	Dgi	Dge	Dg1	wgi	wge	wg1		cedat	wg2							L/cos(beta)	
0	264,9	1240,07	224,4	957,2	69,2	31,88	**8,68**	360	360	55,51	188,75	40,32	**222,82**	**194,88**	0,00	**222,82**	0,40	0,36	1,40	0,8	61236,88	74334,41	0,186	**0,34629**
0	264,9	1240,07	224,4	957,2	49,2	28,01	7,03	360	360	39,47	188,75	40,32	222,82	194,88	0,00	222,82							0,186	
	CX-93	traseu aer																						
	S(LPA)c	S(HPA)c	S(LPA)	S(HPA)	S(x)		de	Dai	Dae	Da1	wai	wae	wa1		primit	wa2								
8	1034	227,55	802,6	178,4	69,2	31,88	**8,68**	360	360	15,52	48,36	219,73	**62,30**	**54,49**	0,00	**62,30**	0,70	3,12	1,40	1,44	14771,21	19712,08	0,186	**0,22934**
8	1034	227,55	802,6	178,4	49,2	28,01	7,03	360	360	11,03	48,36	219,73	62,30	54,49	0,00	62,30							0,186	
	SUPGM varianta 1		traseu gaze evacuare																					
	S(HPG)c	S(LPG)c	S(HPG)	S(LPG)	S(x)		de	Dgi	Dge	Dg1	wgi	wge	wg1		cedat	wg2								
8	264,9	1240,07	217,9	922,3	38,62	22,93	6,74	360	360	31,90	188,75	40,32	229,46	**202,67**	0,00	229,46							0,11714	
8	264,9	1240,07	217,9	922,3	68,05	29,46	9,24	360	360	56,21	188,75	40,32	229,46	202,67	0,00	229,46							0,11714	
8	264,9	1240,07	217,9	922,3	50,77	25,61	7,93	360	360	41,94	188,75	40,32	229,46	202,67	0,00	229,46							0,11714	
8	264,9	1240,07	217,9	922,3	61,06	28,3	**8,63**	360	360	50,44	188,75	40,32	**229,46**	202,67	0,00	229,46	0,04	0,26	1,40	0,5	64724,33	76871,66	0,11714	**0,22918**
	SUPGM varianta 1		traseu aer																					
	S(LPA)c	S(HPA)c	S(LPA)	S(HPA)	S(x)		de	Dai	Dae	Da1	wai	wae	wa1		primit	wa2								
8	1034	227,55	787,9	184,4	38,62	22,93	6,74	360	360	8,82	48,36	219,73	**63,46**	56,05	0,00	**63,46**							0,11714	
8	1034	227,55	787,9	184,4	68,05	29,46	9,24	360	360	15,55	48,36	219,73	63,46	56,05	0,00	63,46							0,11714	
8	1034	227,55	787,9	184,4	50,77	25,61	7,93	360	360	11,60	48,36	219,73	63,46	56,05	0,00	63,46							0,11714	
8	1034	227,55	787,9	184,4	61,06	28,3	**8,63**	360	360	13,95	48,36	219,73	63,46	56,05	0,00	63,46	0,10	3,12	1,40	1	15724,78	20662,15	0,11714	**0,16327**
	SUPGM varianta 2		traseu gaze evacuare																					
	S(HPG)c	S(LPG)c	S(HPG)	S(LPG)	S(x)		de	Dgi	Dge	Dg1	wgi	wge	wg1		cedat	wg2								
8	264,9	1240,07	231,4	1002,9	68,71	33,93	**8,10**	360	360	53,45	188,75	40,32	**216,08**	**190,84**	0,00	**216,08**	0,04	0,26	1,40	0,5	63842,34	78383,82	0,11714	**0,22326**
8	264,9	1240,07	231,4	1002,9	47,92	30,66	6,25	360	360	37,27	188,75	40,32	216,08	190,84	0,00	216,08							0,11714	
	SUPGM varianta 2		traseu aer																					
	S(LPA)c	S(HPA)c	S(LPA)	S(HPA)	S(x)		de	Dai	Dae	Da1	wai	wae	wa1		primit	wa2								
8	1034	227,55	844,1	202,5	68,71	33,93	**8,10**	360	360	14,65	48,36	219,73	**59,23**	**52,32**	0,00	**59,23**	0,10	3,30	1,40	1	14190,86	18711,57	0,11714	**0,15727**
8	1034	227,55	844,1	202,5	47,92	30,66	6,25	360	360	10,22	48,36	219,73	59,23	52,32	0,00	59,23							0,11714	
	SUPGM varianta 3		traseu gaze evacuare																					
	S(HPG)c	S(LPG)c	S(HPG)	S(LPG)	S(x)		de	Dgi	Dge	Dg1	wgi	wge	wg1		cedat	wg2								
8	264,9	1248	231,9	1009,8	68,80	33,5	**8,22**	360	360	53,41	188,75	40,06	**215,61**	**190,43**	0,00	**215,61**	0,04	0,24	1,40	0,5	62680,44	76957,27	0,11714	**0,21852**
8	264,9	1248	231,9	1009,8	48,36	29,45	6,57	360	360	37,54	188,75	40,06	215,61	190,43	0,00	215,61							0,11714	
	SUPGM varianta 3		traseu aer																					
	S(LPA)c	S(HPA)c	S(LPA)	S(HPA)	S(x)		de	Dai	Dae	Da1	wai	wae	wa1		primit	wa2								
8	1040	240,6	850	201,4	68,80	33,5	**8,22**	360	360	14,57	48,08	207,81	**58,82**	**51,95**	0,00	**58,82**	0,10	3,30	1,40	1	13799,29	18195,25	0,11714	**0,14562**
8	1040	240,6	850	201,4	48,36	29,45	6,57	360	360	10,24	48,08	207,81	58,82	51,95	0,00	58,82							0,11714	

	Reynolds	Epsilon/d	Lambda	R [Pa/m]
CX-93				
wg1	37601,197	0,04606936	0,07	61236,884
wg2	42991,481	0,04606936	0,065	74334,407
wa1	31538,906	0,04606936	0,072	14771,214
wa2	23517,48	0,04606936	0,0735	19712,083
SUPGM-1				
wg1	38868,394	0,04634791	0,068	64724,331
wg2	44007,846	0,04634791	0,063	76871,657
wa1	32248,089	0,04634791	0,072	15724,783
wa2	23812,277	0,04634791	0,0738	20662,153

	Reynolds	Epsilon/d	Lambda	R [Pa/m]
SUPGM-2				
wg1	34354,72005	0,04938	0,071	63842,34281
wg2	38897,34246	0,04938	0,068	78383,81791
wa1	28253,81668	0,04938	0,07	14190,85853
wa2	20862,87052	0,04938	0,072	18711,56706
SUPGM-2				
wg1	34765,70132	0,04869	0,071	62680,44238
wg2	39362,66657	0,04869	0,068	76957,26951
wa1	28454,70401	0,04869	0,07	13799,28692
wa2	21011,20752	0,04869	0,072	18195,2545

3.4 MODELING OF FLOW EQUATIONS OF FLUIDS CONSIDERED VISCOUS [97, 98, 99]

In this section are briefly presented the characteristic equations for processes inside of pressure wave compressors, established on the basis of the fundamental principles of physics for the unsteady, three-dimensional, compressible and viscous flow of fluids. It is considered that the effects of viscosity, thermal conductivity and diffusion mass are important due to the consistent variation of fluid pressure and temperature in front of and behind the pressure wave or shock wave front. For an isotropic Newtonian fluid, a complete set of Navier–Stokes equations with variable properties consists of writing the conservation equations of mass, momentum, and energy. The 19 equations are summarized below:

$$\frac{D\rho}{Dt} + \rho\nabla \cdot V = 0 \qquad \text{(1 ec.)} \tag{4.66}$$

$$\rho\frac{\mathrm{DV}}{\mathrm{Dt}} = -\nabla \mathrm{p} + \rho \mathrm{f} + \nabla \cdot \tau \qquad \text{(3 ec.)} \tag{4.67}$$

$$\rho\frac{\mathrm{D}}{\mathrm{Dt}}\left(\mathrm{e} + \frac{1}{2}\boldsymbol{V}\cdot\boldsymbol{V}\right) = \rho\dot{\mathrm{q}}_{\mathrm{gen}} - \nabla\cdot\dot{\mathrm{q}}_{\mathrm{visc}} - \nabla\cdot(\mathrm{pV}) + \rho(\mathrm{f}\cdot\mathrm{V}) + \nabla\cdot(\tau\cdot\boldsymbol{V}) \quad \text{(1 ec.)} \tag{4.68}$$

$$\tau = \mu\left(\nabla \mathrm{V} + \nabla \mathrm{V}^{\mathrm{T}}\right) + \lambda(\nabla\cdot\mathrm{V})\mathrm{I} \qquad \text{(6 ec.)} \tag{4.69}$$

$$\dot{\boldsymbol{q}}_{visc} = \dot{\boldsymbol{q}}_{cond} = -k\nabla\boldsymbol{T} \qquad \text{(3 ec.)} \tag{4.70}$$

$$\dot{\boldsymbol{q}}_{gen} = 0 \qquad \text{(0 ec., neglectable)} \tag{4.71}$$

$$\mu = \mu(\rho, \boldsymbol{T}) \qquad \text{(1 ec.)} \tag{4.72}$$

$$\lambda = \lambda(\rho, \boldsymbol{T}) \qquad \text{(1 ec.)} \tag{4.73}$$

$$k = k(\rho, \boldsymbol{T}) \qquad \text{(1 ec.)} \tag{4.74}$$

$$p = p(\rho, \boldsymbol{T}) \qquad \text{(1 ec.)} \tag{4.75}$$

$$e = e(\rho, \boldsymbol{T}) \qquad \text{(1 ec.)} \tag{4.76}$$

The variables of the differential system above are:

- ρ – density $[kg/m^3]$
- $\boldsymbol{V}$ – velocity, 3 variables $[m/s]$
- p – pressure $[N/m^2]$
- e – internal energy $[J/kg]$
- T – temperature $[K]$
- τ –viscosity forces tensor, 6 variables $[N/m^2]$
- $\boldsymbol{q}_{\mathrm{cond}}$ – heat flow vector, 3 variables $[W/m^2]$
- μ – the first viscosity coefficient $[N.s/m^2$ ori $kg/m.s]$
- λ – 2nd viscosity coefficient $[kg/m.s]$
- k – thermal conductivity $[W/m.K]$

The force applied to the fluid considered in most models is given only by the gravitational field, in this case f = g = gravitational acceleration, considered constant. The result is a differential system with 19

equations and 19 variables that can be determined. To be physically consistent, the system of differential equations and constitutive equations for the thermal conductivity k(ρ,T), the heat flux $\dot{q}_{ht}$, the first viscosity coefficient μ(ρ,T), the second viscosity coefficient λ(ρ,T) and the viscosity tensor τ must respect the Second Principle of thermodynamics. The equations synthesized here are the basis of the software used in the simulation of fluid flow in the PWS and the validation in the virtual research of this paper.

3.5. THEORY OF LINEAR WAVES. PRESSURE WAVES IN PWS

The main processes that occur inside the PWS channels include the formation and propagation of pressure waves, therefore, they are based on the difference between the velocities of the compression or expansion waves and the displacement speed of the contact interface between the air and the combustion gases. Since the equivalent diameter of the channel is much smaller than its length (ratio <<10), the simulation of these non-stationary processes can be conveniently approximated by the one-dimensional approach to the problem [34]. Waves can propagate in media moving with non-zero flow velocities. In Fig. 4.28 is represented the case of the wave that moves with the speed ±w in a medium with the parameters: pressure p1, flow velocity u1 and sound speed a1 (the parameters marked with index 1 represent the environment "in front" of the wave) and modify the environment parameters in p2, u2 and a2 (the index 2 is noted for the "back" of the wave). The speed w is considered relative to the fluid in which it propagates and the + and - signs to the type of wave (overpression or underpression).

The continuity, momentum and energy conservation equations can be applied to the stationary control volume [61], writing the velocity ws as a function of w, u_1 and u_2:

$$\rho_1 \cdot w = \rho_2 \cdot [w \pm (u_1 - u_2)] \tag{4.96}$$

$$p_1 + \rho_1 \cdot w^2 = p_2 + \rho_2 \cdot [w \pm (u_1 - u_2)]^2 \tag{4.97}$$

$$h_1 + \frac{w^2}{2} = h_2 + \frac{[w \pm (u_1 - u_2)]^2}{2} \tag{4.98}$$

The equations can be transformed as a function of the Mach number of the wave $M = \frac{w}{a_1}$ or depending on the pressure ratio Π_s [48, 61]:

$$\frac{u_2 - u_1}{a_1} = \pm \frac{2}{k+1}\left(M - \frac{1}{M}\right) \tag{4.99}$$

$$or \quad \frac{u_2 - u_1}{a_1} = \pm \frac{\Pi_s - 1}{k} \sqrt{\frac{2 \cdot k}{\Pi_s (k+1) + (k-1)}} \tag{4.100}$$

$$M = \sqrt{1 + \frac{k+1}{2k}(\Pi_s - 1)} \tag{4.101}$$

$$\left(\frac{a_2}{a_1}\right)^2 = 1 + \frac{2(k-1)}{(k+1)^2}\left[k \cdot M^2 - \frac{1}{M^2} - k + 1\right] \tag{4.102}$$

$$\frac{p_2}{p_1} = 1 + \frac{2k}{k+1}(M^2 - 1) \tag{4.103}$$

$$M_s = \frac{w_s}{a_1} = \sqrt{1 + \frac{k+1}{2k}(\Pi_s - 1)} \tag{4.104}$$

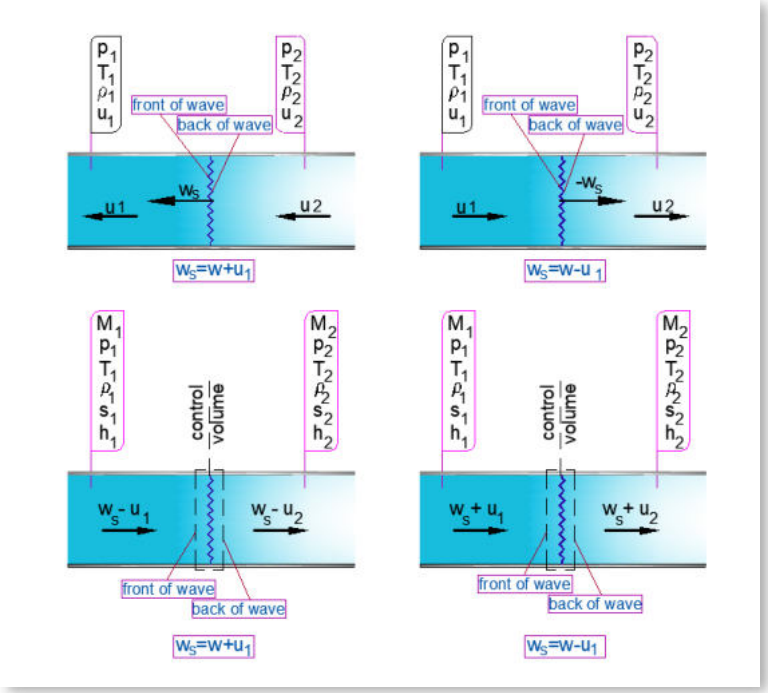

Figure 4.28 – Fluid parameters when flowing through a pressure wave, in a stationary coordinate system (top) and in a mobile coordinate system fixed to the wave (bottom)

a) wave that moves in the same direction as the fluid b) wave that moves with the opposite sign

From equation (4.104) it can be seen that the propagation speed of the shock wave increases with the increase of its pressure ratio. The induced flow velocity also increases, but the Mach number for the flow remains subsonic. The Mach number for the shock wave decreases due to the increase in temperature due to compression (the conversion of kinetic energy into compensating enthalpy due to the drastic decrease in fluid velocity) [48, 99].

3.6. CRITICAL SECTION. THE CHOKED FLOW MODEL

The study of the phenomena that take place inside a wave rotor is based on certain assumptions, including the fact that the channel openings occur instantaneously and are sufficiently wide [39]. In reality, when the channels gradually open to high-velocity ports, curved waves are initially produced in the corner where the fluid begins to penetrate, which are then reflected by the opposite wall, after which they form a train of compression waves that propagate approx. normal to the channel wall [39]. The flow from the ports to the rotor, through the channels can be assimilated to the flow in convergent-divergent nozzles (Fig. 4.33), for which, when the channels are fully opened in front of the port passage, the flow is

subsonic. According to the theory of converging nozzles, the critical section - the limit section for producing shock waves - is constantly "positioned" in the area of the minimum section where the flow is sonic, until the flow section exceeds the value at which it can be considered a nozzle.

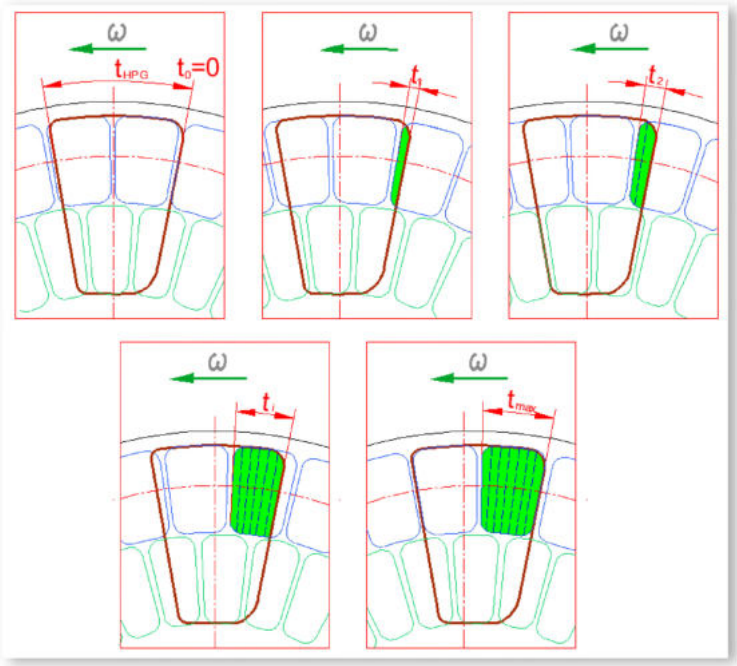

Figure 4.32 – Gradual opening of a channel to the HPG port

In Fig. 4.32 is represented the gradual opening of a channel towards the port, considered from the outer row of channels, and the exposed surface of the channel (colored in green) can be observed at different times denoted ti, starting with $t_0=0$, when the channel is completely closed. The exposed surface of a cell at the gradual opening in front of the HPG port at the PWS is shown for example in Fig.4.34.

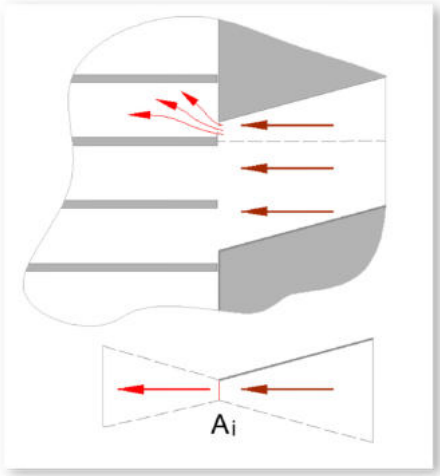

Figure 4.33 – Partial channel opening and association with flow in a convergent-divergent nozzle

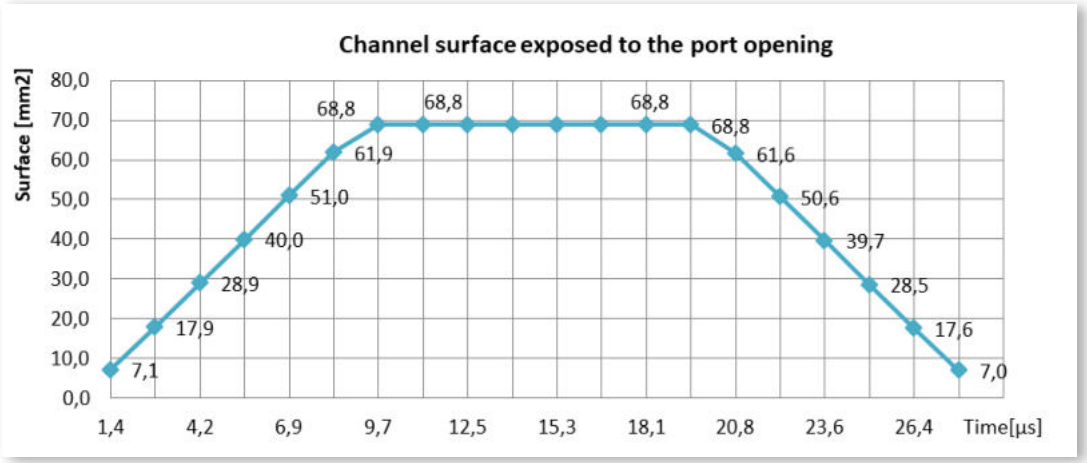

Figure 4.34 – Time variation of the channel surface at the opening in front of the exhaust gas inlet port

Modeling the flow of fluids from the port to the rotor channels, at their gradual opening near the port window, can be achieved by writing the equations that govern the flow through a convergent-divergent nozzle (Fig.4.33). In the minimum section denoted Ai, the maximum speed to which the fluid can be accelerated, which is the speed of sound, is reached. Thus, for the gas considered ideal, with the ratio of specific heats constant, the equations of the stagnation-to-static parameters can be written [99]:

$$\frac{T_0}{T} = 1 + \left(\frac{k-1}{2}\right) M^2 \qquad (4.117)$$

$$\frac{p}{p_0} = \left[1 + \left(\frac{k-1}{2}\right) M^2\right]^{\frac{k}{k-1}} \qquad (4.118)$$

$$\frac{\rho_0}{\rho} = \left[1 + \left(\frac{k-1}{2}\right) M^2\right]^{\frac{1}{k-1}} \qquad (4.119)$$

The fluid flow through a nozzle depends on the Mach number and stagnation properties, and for stationary conditions, it remains constant and can be calculated with the equation (4.120):

$$\dot{m} = \frac{A \cdot M \cdot p_0 \sqrt{\frac{k}{RT_0}}}{\left[1 + \frac{(k-1)}{2} M^2\right]^{\frac{k+1}{2(k-1)}}} \qquad (4.120)$$

In the minimum section the flow is sonic, so the Mach number is unity (M=1) and the fluid properties reach "critical" values, denoted here by *:

$$\frac{T^*}{T_0} = \frac{2}{k+1} \qquad (4.121)$$

$$\frac{p^*}{p_0} = \left(\frac{2}{k+1}\right)^{\frac{k}{k-1}} \qquad (4.122)$$

$$\frac{\rho^*}{\rho_0} = \left(\frac{2}{k+1}\right)^{\frac{1}{k-1}} \qquad (4.123)$$

The maximum flow for choked flow of the fluid stream can be calculated with [99]:

$$\dot{m}_{max} = A^* \cdot p_0 \cdot \left(\frac{2}{k+1}\right)^{\frac{k+1}{2(k-1)}} \sqrt{\frac{k}{RT_0}} \qquad (4.124)$$

where the critical area A* can be read from tables in the literature or calculated with:

$$\frac{A}{A^*} = \frac{1}{M} \cdot \left[\frac{2+(k-1)M^2}{k+1}\right]^{\frac{k+1}{2(k-1)}} \qquad (4.125)$$

If the critical values of the state parameters, the critical section and the maximum flow in the HPG and HPA ports are calculated, for the CX-93 and for the PWSMG variants, it is observed, for example, that, for the CX-93, the critical section is approx. 55.8 % of the surface of the channel. Taking into account that the maximum velocity in this section is the speed of sound, it follows that, at the opening of the channel from t_0 to t_i=t*, the velocity of the fluid is the speed of sound, after which it decreases to the value lower than the speed of sound. The disturbance produced at the opening of the channel can accelerate the fluid and, thus, it can further develop a normal wave in the channel, which will cause a sudden decrease in the speed at the subsonic level and an increase in pressure and temperature [99]. The approximation of the events in the port area with the model of the flow through the nozzles provides an image of their evolution. In reality, sudden section variations induce large pressure losses, especially in the area of the small sections at the beginning of the opening and the end of the channels closing, which can produce shock waves and interference of their fronts, much more difficult to analyze and quantify theoretically.

3.7 MODELING OF THE AVL BOOST VIRTUAL TEST RIG

The construction of the virtual model aims to use the AVL Boost virtual stand for the simulation of the processes that occur inside the PWS, which allows in the first phase to validate the model by simulating the operation of the Comprex CX-93 supercharger and comparing the results with the experimental ones reported in the literature, and in the second phase, the use of the model for behavior analysis and validation in a virtual medium of the new supercharger with modified geometry.

Fig.4.35 shows the schematic model of the virtual "test rig", which includes: the virtual model of the engine (the PDC1 compressor for simulating combustion gas parameters), the virtual model of the Comprex CX-93 supercharger, system boundaries, connecting pipes (1...14), plenum (PL1), restrictions (R1...R5) and measurement points (MP1...MP15). The virtual model has the possibility to modify some predefined characteristics of the PWS in terms of dimensions and geometric positions of the component elements (Fig. 4.37, 38).

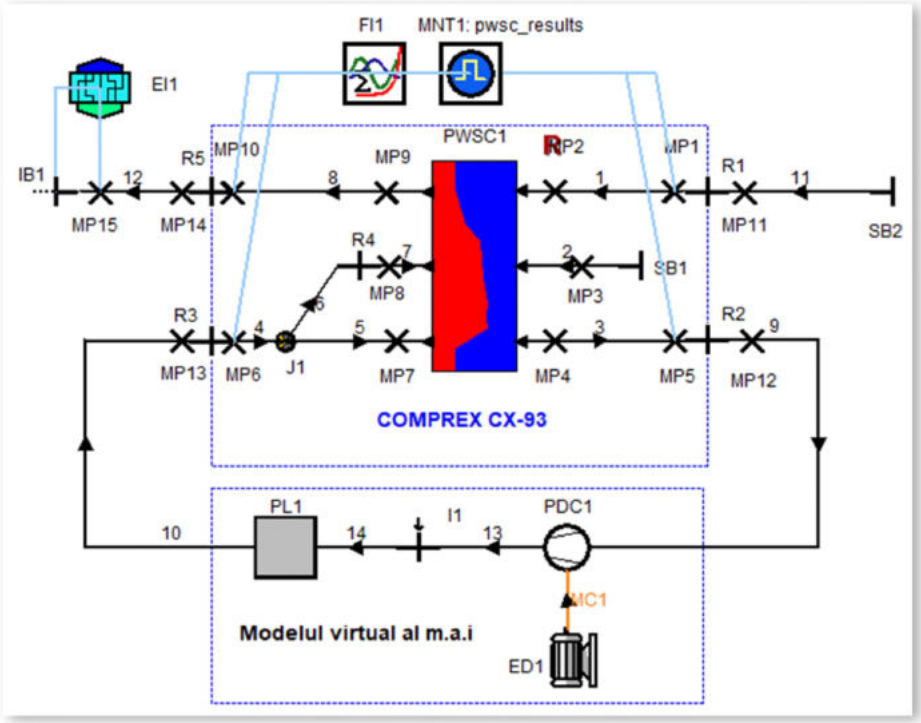

Figure 4.35. The virtual test stand of the COMPREX CX-93 supercharger

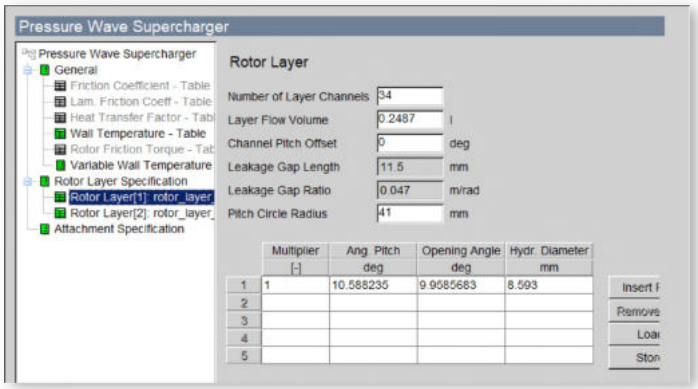

Figure 4.37 – Geometric characteristics of the first row of cells

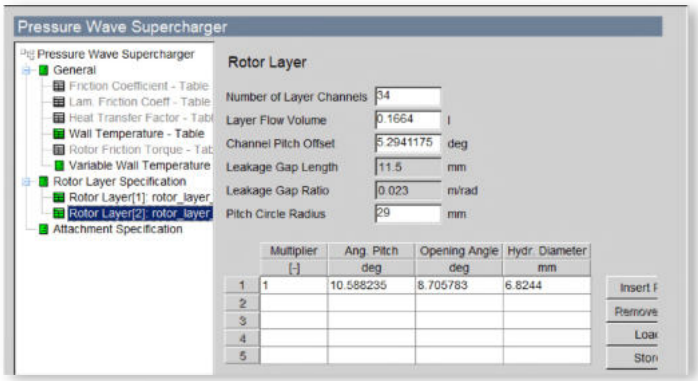

Figure 4.38 – Geometric characteristics of the second row of cells

3.8 VIRTUAL EXPERIMENTAL RESEARCH METHODOLOGY

The simulation of the operation of the PWSMG and the validation of the results were carried out in two stages: (1) simulation of the PWS CX-93 operation on the modeled test rig and comparing the results obtained with those reported in the literature with the aim of validating the AVL Boost model used; (2) simulation of the new PWSMG operation and analysis of the obtained results.

3.8.1 VIRTUAL EXPERIMENTAL SIMULATION AND VALIDATION FOR THE CX-93 MODEL

The first stage was to simulate the operation of the Comprex CX-93 using as input data: atmospheric air parameters (LPA inlet port) and exhaust gas state parameters (HPG inlet port), with values reported in literature: pressure, temperature, mass flow rates. Two simulations were carried out, for two sets of input data, the data obtained in 15 measurement points being presented in Tables 5.1 and 5.2 for set 1 and set 2 respectively. The points of interest are MP 1(2) for LPA atmospheric air, MP 5(4) for HPA compressed air, MP 6(7) for HPG combustion gas inlet and MP 10(9) for LPG exhaust gas outlet.

Table 5.1 – Data at measurement points for Comprex CX-93 parameter set 1

MEASURINGPOINTS: Average Values

Mp. nr.	Pipe nr.	Location [mm]	Diameter [mm]	Pressure [bar]	Temp. [K]	Ms.Temp. [K]	Velo. [m/s]	Massflow [g/s]	Massflow [g/cycle]	To.Ent.f. [kJ/s]	To.Ent.f. [kJ/cyc.]	Mach. [-]	Wtemp. [K]	Converg. [-]
1	1	10.0000	60.9500	0.9487	292.2	292.2	44.5	146.5963	0.5864	-0.740	-0.0030	0.13	373.1	0.663E-07
2	1	140.0000	47.3000	0.9273	290.4	290.4	75.0	146.5964	0.5864	-0.740	-0.0030	0.22	373.1	0.388E-07
3	2	7.0000	33.0000	1.9141	442.6	0.0	0.0	0.0000	0.0000	0.000	0.0000	0.00	423.2	0.441E-04
4	3	0.0000	25.0000	1.7569	391.4	391.6	137.9	105.9212	0.4237	11.008	0.0440	0.35	423.1	0.998E-07
5	3	90.0000	47.5000	1.8972	402.5	402.5	36.7	105.9283	0.4237	11.217	0.0449	0.09	423.1	0.238E-06
6	4	10.0000	52.4000	2.0725	1023.4	1023.4	70.8	107.8280	0.4313	85.748	0.3430	0.11	773.1	0.102E-06
7	5	30.0000	29.9000	2.0274	1018.0	1018.0	133.9	65.2183	0.2609	51.861	0.2074	0.22	773.1	0.414E-07
8	7	20.0000	26.4000	1.9156	1019.7	1019.7	118.7	42.6154	0.1705	33.888	0.1356	0.19	773.2	0.103E-06
9	8	0.0000	52.0000	1.0042	753.8	753.9	150.4	148.4580	0.5938	73.072	0.2923	0.28	573.1	0.126E-05
10	8	85.0000	62.2895	1.0312	760.8	760.8	103.2	148.4577	0.5938	73.324	0.2933	0.19	573.1	0.706E-07
11	11	280.0000	62.0000	0.9495	292.2	292.2	42.9	146.5908	0.5864	-0.740	-0.0030	0.13	313.2	0.630E-07
12	9	20.0000	50.0000	1.8994	403.7	403.7	32.9	105.9293	0.4237	11.339	0.0454	0.08	433.2	0.388E-06
13	10	280.0000	53.0000	2.0735	1023.7	1023.7	69.1	107.8318	0.4313	85.773	0.3431	0.11	1023.1	0.180E-06
14	12	20.0000	63.5000	1.0331	759.9	759.9	98.8	148.4625	0.5939	73.098	0.2924	0.18	298.0	0.699E-07
15	12	380.0000	63.5000	1.0321	736.0	736.0	95.8	148.4582	0.5938	69.121	0.2765	0.18	298.0	0.558E-07

Table 5.2 – Data at measurement points for Comprex CX-93 parameter set 2

MEASURINGPOINTS: Average Values

Mp. nr.	Pipe nr.	Location [mm]	Diameter [mm]	Pressure [bar]	Temp. [K]	Ms.Temp. [K]	Velo. [m/s]	Massflow [g/s]	Massflow [g/cycle]	To.Ent.f. [kJ/s]	To.Ent.f. [kJ/cyc.]	Mach. [-]	Wtemp. [K]	Converg. [-]
1	1	10.0000	60.9500	0.9503	292.3	292.3	41.2	136.0513	0.5442	-3.686	-0.0027	0.12	373.1	0.114E-07
2	1	140.0000	47.3000	0.9320	290.8	290.8	69.4	136.0509	0.5442	-3.686	-0.0027	0.20	373.1	0.784E-08
3	2	7.0000	33.0000	1.8187	419.4	0.0	0.0	0.0000	0.0000	3.000	0.0000	0.00	423.1	0.102E-03
4	3	0.0000	25.0000	1.9306	398.0	398.4	116.4	99.1401	0.3966	10.711	0.0428	0.29	423.2	0.133E-06
5	3	90.0000	47.5000	2.0906	406.7	406.7	31.5	99.1577	0.3966	10.909	0.0436	0.08	423.2	0.179E-07
6	4	10.0000	52.4000	2.1412	1023.5	1023.5	64.1	100.9248	0.4037	80.215	0.3209	0.10	773.2	0.220E-07
7	5	30.0000	29.9000	2.0852	1017.0	1017.0	139.8	70.1227	0.2805	55.730	0.2229	0.23	773.2	0.167E-07
8	7	20.0000	26.4000	1.8589	1022.0	1322.0	88.2	30.8143	0.1233	24.486	0.0979	0.14	773.1	0.379E-07
9	8	0.0000	52.0000	1.0083	756.2	756.2	139.5	137.8213	0.5513	67.984	0.2719	0.26	573.1	0.456E-07
10	8	85.0000	62.2895	1.0313	762.4	762.4	95.9	137.8205	0.5513	68.216	0.2729	0.18	573.1	0.290E-07
11	11	280.0000	62.0000	0.9510	292.4	292.4	39.8	136.0501	0.5442	3.686	0.0027	0.12	313.2	0.616E-08
12	9	20.0000	50.0000	2.0923	408.1	408.1	28.3	99.1569	0.3966	11.045	0.0442	0.07	443.2	0.131E-06
13	10	280.0000	53.0000	2.1420	1023.7	1023.7	62.6	100.9240	0.4037	80.234	0.3209	0.10	1023.2	0.779E-07
14	12	20.0000	63.5000	1.0329	761.4	761.4	92.0	137.8214	0.5513	68.004	0.2720	0.17	298.0	0.199E-07
15	12	380.0000	63.5000	1.0321	737.3	737.3	89.1	137.8227	0.5513	64.299	0.2572	0.17	298.0	0.443E-08

In Fig. 5.3 are represented the pressure variations of the working fluids, noting that the pressure values of the high-pressure fluids converge towards 1.89 bar (HPA) and 2.07 bar (HPG) for data set 1 (simulation 1) and, respectively, towards 2 .09 bar (HPA) and 2.14 bar (HPG) for data set 2 (simulation 2).

Fig.5.5 shows the fluid velocities in the port area, the values being read at measurement points 2, 4, 7 and 9. The values of interest are: the exhaust gas velocity at the entrance to the CX-93 (MP7), located at 135...140 m/s for both simulations and compressed air velocity (MP4) stabilized at ~137 m/s in the first simulation and 116 m/s in the second. It is observed that these values are kept in the subsonic zone, this being one of the optimal operating conditions for the pressure wave supercharger.

Table 5.3 summarizes the values resulting from the simulation of Comprex CX-93 operation on the AVL Boost virtual stand.

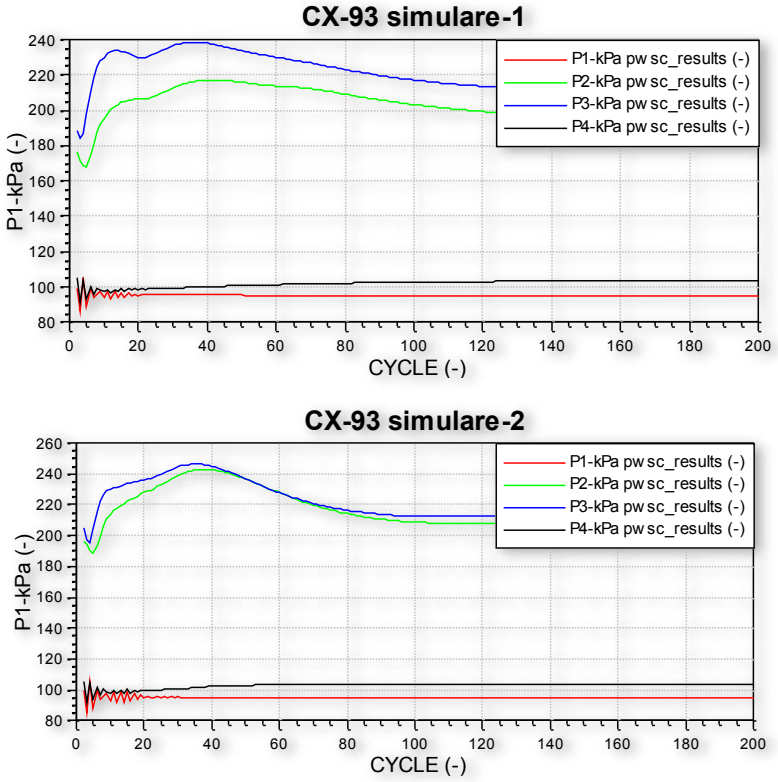

Figure 5.3 – Variation of pressures for data set 1 (top figure) and data set 2 (bottom figure) for CX-93

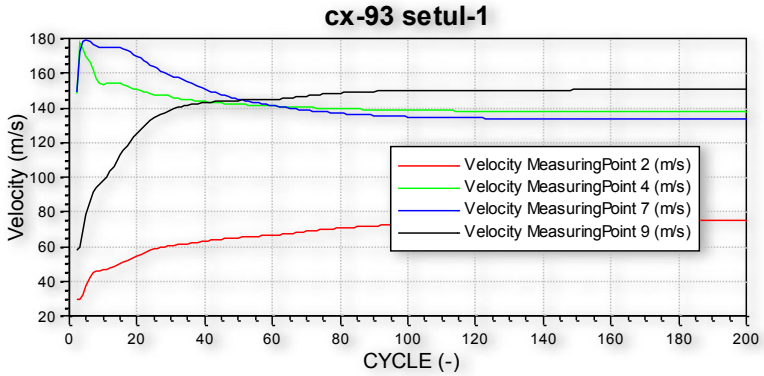

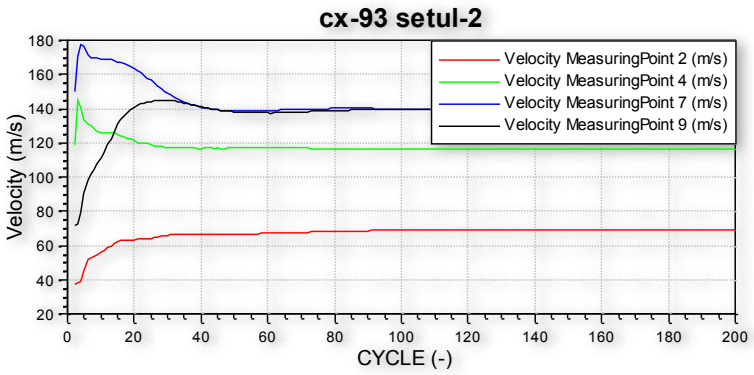

Figure 5.5 – Variation of fluid velocities for data set 1 (simulation 1) and data set 2 (simulation 2) for CX-93

Table 5.3 – Results of the operation simulation on the AVL Boost virtual stand, experimental data reported in the literature and relative errors

Experimental data reported in literature								
	Smith [54]				Pohorelsky et al. [47]			
Parameters	HPG	HPA	LPG	LPA	HPG	HPA	LPG	LPA
Pression [bar]	1,845	1,676	1,046	1,0032	2,1	1,95	1	1
Temp. [K]	548	372	471	306	900	400	595	393
Mass flow [g/s]	98,8	98,8	103	103	100	83,3	150	147

Simulation results for CX-93								
	Virtual model AVL Boost				Virtual model AVL Boost			
	CX-93 simulare 1				CX-93 simulare 2			
Parameters	HPG	HPA	LPG	LPA	HPG	HPA	LPG	LPA
Pression [bar]	2,027	1,75	1,042	0,9487	2,14	1,98	1,03	0,95
Temp. [K]	1018	402,5	761	292	1023	406	762	292
Mass flow [g/s]	107,8	105,9	147,5	146,6	101	99	138	136

Relative errors [%]								
	Simulation 1 vs. Smith [54]				Simulation 2 vs. Pohorelsky [47]			
Parameters	HPG	HPA	LPG	LPA	HPG	HPA	LPG	LPA
Pression [bar]	-9,9	-4,4	0,4	5,4	-1,9	-1,5	-3,0	5,0
Temp. [K]	-85,8	-8,2	-61,6	4,6	-13,7	-1,5	-28,1	25,7
Mass flow [g/s]	-9,1	-7,2	-43,2	-42,3	-1,0	-18,8	8,0	7,5

The results of the simulations are analyzed and compared with results obtained experimentally and reported in the literature. It is observed that, regarding the pressure of the combustion gases at the entrance to the CX-93 rotor, values of 2.0...2.1 bar were recorded, comparable to the experimental ones of 1.98...2.1 bar, the calculated relative error being a maximum of 9.9%. Comparing the results obtained in

terms of compressed air pressure, it is observed that it recorded values of 1.7...1.98 bar in the simulation, while the experimental values were at 1.6...1.95 bar, the maximum relative error being ~ 4.4 %. Regarding the temperature values, the reported values are very different, the experiments being carried out without considering the temperature, therefore, they cannot be analyzed by comparison. Regarding the flows, it is observed that the major deviations are in the case of "Simulation vs. Smith [54]" at the fresh air intake and exhaust gas flow rates, but this shows that the EGR phenomenon is present, which is taken into account in the simulation on the virtual test rig.

Thus, accepting a maximum relative error of 10%, it can be concluded that the simulation for the CX-93 provided comparable results to the experimental ones reported in the literature, and the results validate the AVL Boost model and justify its further use as a tool for simulation and analysis of the functioning of the PWSMG proposed in this paper.

3.8.2 SIMULATION AND EXPERIMENTAL VALIDATION OF THE NEW PWSMG

The simulation of the new PWSMG operation was carried out on the virtual test rig modeled and validated for the CX-93, by replacing the supercharger with the new configuration, and with adjustment of the dimensional characteristics: number of channels per row (36 channels on 2 rows), the new length of the rotor (L=58 mm), equivalent diameters, the angle between the HPG and compressed HPA ports reduced by 8° (equivalent to the axial inclination of the channels of the new PWSMG). The constructive details of the virtual test bench and the dimensional values of PWSMG are presented in Fig. 5.10...5.13.

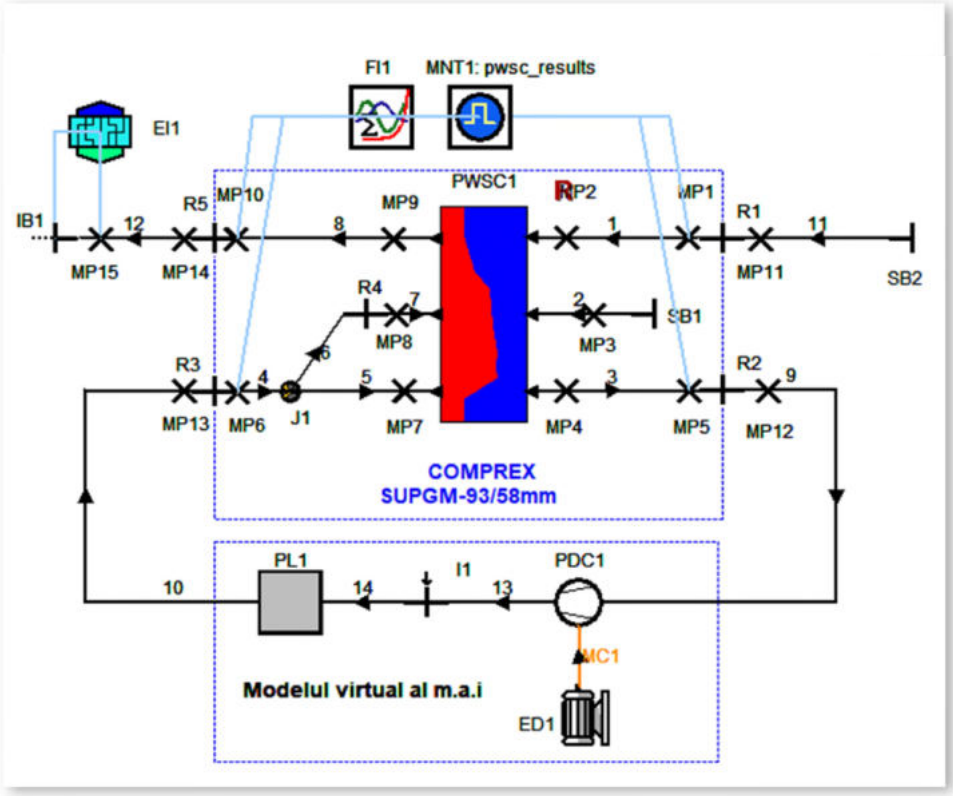

Figure 5.10 – AVL Boost virtual test rig for simulating the operation of the new PWSMG

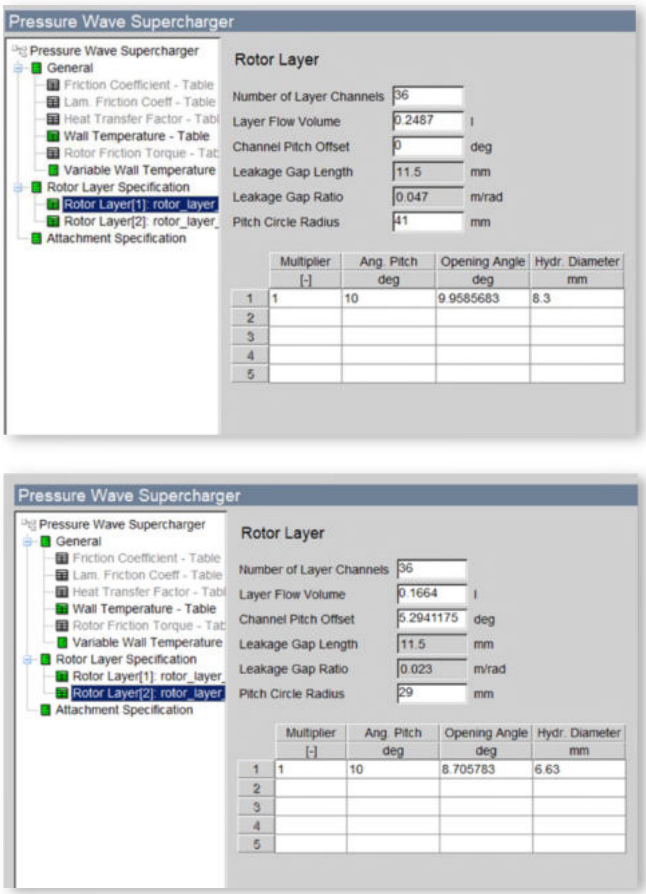

Figure 5.12 – Geometric changes for row 1 (top) and 2 (bottom) of cells according to PWSMG

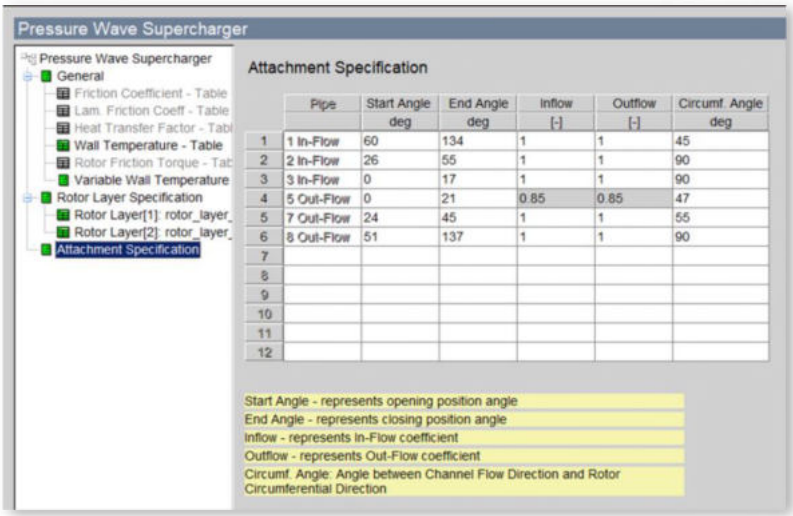

Figure 5.13 – Geometric changes according to PWSMG

The simulation on the AVL-Boost stand consisted of: (1) establishing two sets of input data according to the objectives established for the new PWSMG and performing two simulations whose results will be analysed to validate the new configuration PWSMG and (2) running a 3rd simulation, with

data similar to those of the CX-93 (exhaust gas pressure and flow rates) which enable comparative analysis with the experimental data reported in the literature for the CX-93.

Tables 5.4 and 5.5 show the average values of the parameters of the first two simulations, measured at the measurement points M 1... M 15.

Table 5.4 – Data results in the measurement points M1...M15 of the stand, data set 1

MEASURINGPOINTS: Average Values

Mp. nr.	Pipe nr.	Location [mm]	Diameter [mm]	Pressure [bar]	Temp. [K]	Ms.Temp. [K]	Velo. [m/s]	Massflow [g/s]	Massflow [g/cycle]	To.Ent.f. [kJ/s]	To.Ent.f. [kJ/cyc.]	Mach. [-]	Wtemp. [K]	Converg. [-]
1	1	10.0000	60.9500	0.9528	292.5	292.5	35.5	117.3522	0.4694	-0.592	-0.0024	0.10	373.2	0.232E-06
2	1	140.0000	47.3000	0.9394	291.4	291.4	59.5	117.3514	0.4694	-0.592	-0.0024	0.17	373.2	0.213E-06
3	2	7.0000	33.0000	1.6176	945.4	0.0	0.0	0.0000	0.0000	0.000	0.0000	0.00	423.1	0.406E-03
4	3	0.0000	25.0000	2.0842	547.4	547.8	215.3	140.3107	0.5612	39.124	0.1565	0.46	423.2	0.128E-06
5	3	90.0000	47.5000	2.3820	570.7	570.7	54.9	140.3770	0.5615	39.433	0.1577	0.12	423.2	0.362E-06
6	4	10.0000	52.4000	2.4357	1023.7	1023.7	79.8	142.8950	0.5716	114.263	0.4571	0.13	773.2	0.141E-06
7	5	30.0000	29.9000	2.2289	1002.4	1002.4	239.2	130.1928	0.5208	104.091	0.4164	0.39	773.2	0.205E-06
8	7	20.0000	26.4000	1.7556	1025.9	1025.9	38.8	12.7037	0.0508	10.158	0.0406	0.06	773.1	0.396E-06
9	8	0.0000	52.0000	0.9944	847.5	847.5	137.5	119.6232	0.4785	71.861	0.2874	0.24	573.2	0.705E-07
10	8	85.0000	62.2895	1.0140	853.3	853.3	94.7	119.6223	0.4785	72.062	0.2882	0.17	573.2	0.439E-07
11	11	280.0000	62.0000	0.9533	292.6	292.6	34.2	117.3532	0.4694	-0.592	-0.0024	0.10	313.2	0.251E-06
12	9	20.0000	50.0000	2.3868	565.9	565.9	48.6	140.3827	0.5615	38.677	0.1547	0.10	433.2	0.535E-07
13	10	280.0000	53.0000	2.4372	1024.2	1024.2	78.0	142.8949	0.5716	114.316	0.4573	0.13	1023.2	0.792E-07
14	12	20.0000	63.5000	1.0154	852.0	852.0	90.8	119.6172	0.4785	71.832	0.2873	0.16	298.0	0.321E-07
15	12	380.0000	63.5000	1.0148	823.3	823.3	87.8	119.6201	0.4785	67.868	0.2715	0.16	298.0	0.433E-07

Table 5.5 – Data results in the measurement points M1...M15 of the stand, data set 2

MEASURINGPOINTS: Average Values

Mp. nr.	Pipe nr.	Location [mm]	Diameter [mm]	Pressure [bar]	Temp. [K]	Ms.Temp. [K]	Velo. [m/s]	Massflow [g/s]	Massflow [g/cycle]	To.Ent.f. [kJ/s]	To.Ent.f. [kJ/cyc.]	Mach. [-]	Wtemp. [K]	Converg. [-]
1	1	10.0000	60.9500	0.9254	290.1	290.1	78.3	253.5634	1.0143	-1.280	-0.0051	0.23	373.1	0.437E-07
2	1	140.0000	47.3000	0.8529	283.7	283.7	137.8	253.5622	1.0142	-1.280	-0.0051	0.41	373.1	0.346E-07
3	2	7.0000	33.0000	2.1834	581.6	0.0	0.0	0.0000	0.0000	0.000	0.0000	0.00	423.1	0.126E-04
4	3	0.0000	25.0000	1.5762	382.8	383.0	226.6	159.7409	0.6390	17.823	0.0713	0.58	423.1	0.196E-06
5	3	90.0000	47.5000	1.9455	409.1	409.1	54.9	159.7814	0.6391	18.145	0.0726	0.14	423.1	0.276E-06
6	4	10.0000	52.4000	2.0686	1023.3	1023.3	107.0	162.6491	0.6506	129.863	0.5195	0.17	773.1	0.765E-07
7	5	30.0000	29.9000	1.9909	1013.8	1013.8	184.6	88.6958	0.3548	70.811	0.2832	0.30	773.1	0.113E-06
8	7	20.0000	26.4000	1.9682	1011.7	1011.6	199.1	73.9639	0.2959	59.050	0.2362	0.32	773.1	0.654E-07
9	8	0.0000	52.0000	0.9468	672.4	672.4	245.6	256.1300	1.0245	107.777	0.4311	0.48	573.1	0.859E-07
10	8	85.0000	62.2895	1.0301	689.7	689.7	161.5	256.1331	1.0245	108.209	0.4328	0.31	573.1	0.633E-07
11	11	280.0000	62.0000	0.9279	290.3	290.3	75.4	253.5787	1.0143	-1.280	-0.0051	0.22	313.1	0.554E-07
12	9	20.0000	50.0000	1.9505	410.7	410.7	49.2	159.7782	0.6391	18.349	0.0734	0.12	443.1	0.153E-06
13	10	280.0000	53.0000	2.0710	1023.8	1023.8	104.4	162.6537	0.6506	129.902	0.5196	0.17	1023.1	0.123E-06
14	12	20.0000	63.5000	1.0356	689.6	689.6	154.4	256.1343	1.0245	107.882	0.4315	0.30	298.0	0.446E-07
15	12	380.0000	63.5000	1.0322	669.5	669.5	150.4	256.1379	1.0246	102.165	0.4087	0.29	298.0	0.464E-07

Fig.5.16 shows the pressure variations of the working fluids, noting that the values for LPA and LPG fluids are approximately constant and have the value of the ambient environment. The HPA and HPG fluid pressures show a peak value of 2.6 bar at the beginning of the simulations, after which the values converge towards ~2.4 bar (simulation 1) and ~2.0 bar (simulation 2). The symbols for the parameters of each fluid are:

- 1 (red color) for fresh air intake (LPA);
- 2 (green color) for compressed air (HPA);
- 3 (blue color) for exhaust gases entering the rotor (HPG);
- 4 (black color) for exhaust gases leaving the rotor (LPG).

From Fig.5.16 a comparison can be made on the behavior of the PWSMG in case of higher exhaust gas pressures - 2.4 bar set for simulation 1 compared to 2.0 bar for simulation 2, concluding that the operation is more stable in terms of pressure, with smaller variations in case 1 and with better values of the pressure ratio (P2/P1) of ~2.3 (simulation 1) and 2.0 (simulation 2), respectively. This result shows that PWSMG is better suitable for engines with higher values of the combustion gas pressure and pressure of the compressed air.

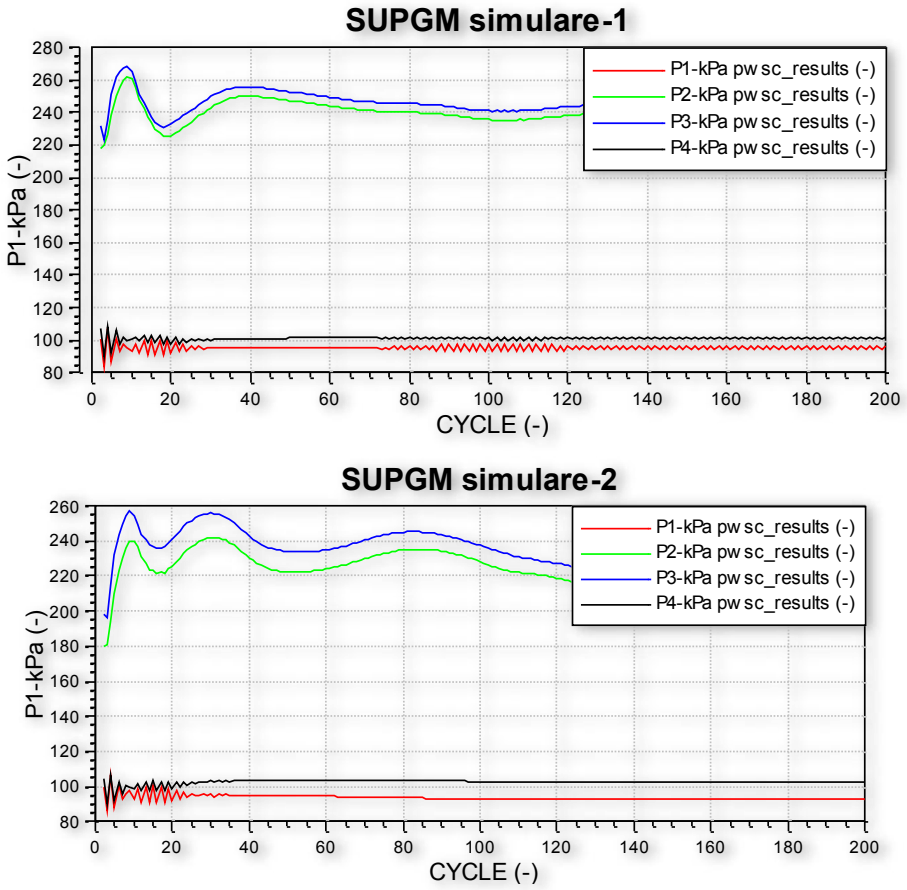

Figure 5.16 – Variation of working fluid pressure for data set 1 (simulation 1) and data set 2 (simulation 2) for PWSMG

Fig.5.18 shows the fluid velocities in the port area, the values being read at measurement points 2, 4, 7 and 9. The values of interest are: the velocity of exhaust gases at the entrance to the PWSMG (MP7), located at ~240 m/s for the first simulation and at ~190 m/s for simulation 2 and the compressed air velocity (MP4) stabilized at ~210 m/s in the first simulation and 230 m/s in the second. It is observed that these values are kept in the subsonic zone, this being one of the optimal operating conditions for the pressure wave supercharger.

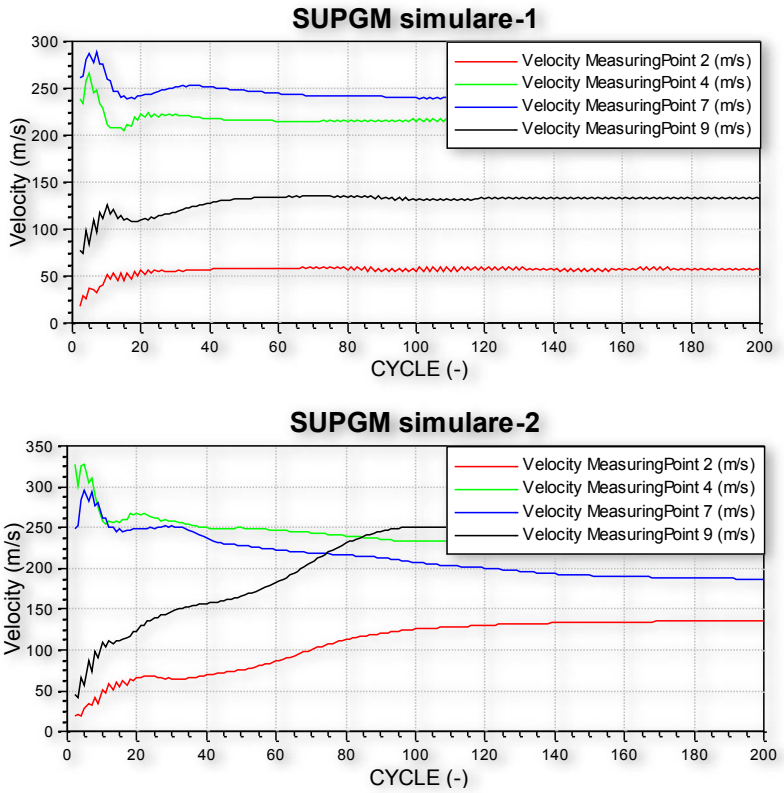

Figure 5.18 – Variation of working fluid velocities for simulation 1 and simulation 2 for PWSMG

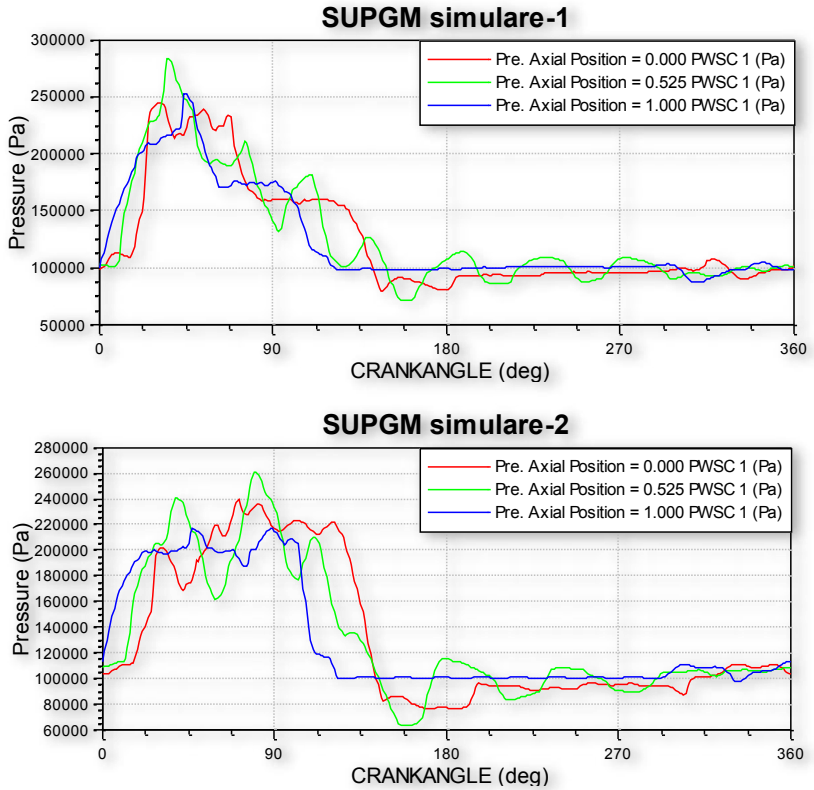

Figure 5.20 – Pressure variation in the rotor channels in simulation 1 and 2 for PWSMG

Fig. 5.20 and 5.21 show the pressure and speed variations along the rotor channels at the hot end (gas inlet – represented in blue), in the middle of the channel (represented in green) and at the cold end (compressed air outlet – represented in red). The pressure peaks are 2.5...2.6 bar in both simulations, for the hot end. At the cold end, the pressure increases due to the pressure waves propagated in the channel and the compressed air flows into the open port, after which it closes and the pressure decreases favoring the intake of fresh air into the channel. The compressed air pressure reaches peak values of 2.45 bar and 2.35 bar, respectively. Velocity variations do not indicate supersonic values for these data sets.

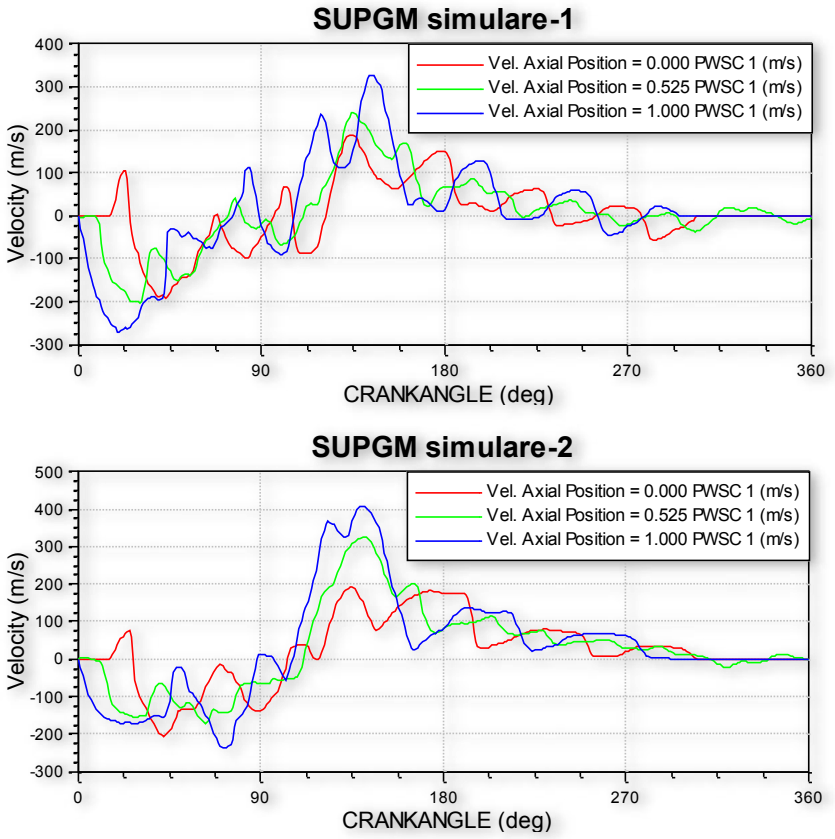

Figure 5.21 – Velocity variation in the rotor channels at different positions of the measurement points for data set 1 (simulation 1) and data set 2 (simulation 2) for PWSMG

The variation of velocities inside the channels (Fig.5.21) shows negative or positive values as a function of the direction in which the fluid moves. The variation curves at the end of the HPG, represented in blue, show how the velocity increases when the channel opens to the gas port, decreases to zero when the channel closes, followed by the acceleration of the fluid as compression waves appear when opening to the gas outlet port low LPG pressure, the decrease in speed with the flow of gases in this port and the "standing still" before resuming the processes in the next cycle. The maximum speed in the channels reaches peak values of 330m/s and 310m/s, thus noting that, including inside the channels, the flow is subsonic.

3.8.3 SIMULATION OF PWSMG OPERATION WITH SIMILAR CX-93 INPUT DATA

In order to analyze the data by comparison with CX-93 and validate the PWSMG model, a third simulation was carried out, with input data similar to the CX-93: exhaust gas pressure at the PWSMG entrance of 2.1 bar, gas mass flow of ~100 g/s, and the rotor speed of 12950 rot/min [47, 57]. The simulation returned the following results, presented in Table 5.6:

Table 5.6 - Data results at measurement points M1...M15 of the stand, data set 3 for PWSMG

MEASURINGPOINTS: Average Values

Mp. nr.	Pipe nr.	Location [mm]	Diameter [mm]	Pressure [bar]	Temp. [K]	Ms.Temp. [K]	Velo. [m/s]	Massflow [g/s]	Massflow [g/cycle]	To.Ent.f. [kJ/s]	To.Ent.f. [kJ/cyc.]	Mach. [-]	Wtemp. [K]	Converg. [-]
1	1	10.0000	60.9500	0.9521	292.5	292.4	40.3	133.2370	0.3087	-0.661	-0.0015	0.12	373.2	0.217E-03
2	1	140.0000	47.3000	0.9375	291.2	291.2	65.4	129.2848	0.2995	-0.630	-0.0015	0.19	373.2	0.175E-03
3	2	7.0000	33.0000	1.4061	648.7	0.0	-0.0	0.0000	0.0000	0.000	0.0000	-0.00	423.2	0.762E+03
4	3	0.0000	25.0000	1.7681	423.1	423.9	143.3	102.4643	0.2374	14.099	0.0327	0.35	423.1	0.563E-04
5	3	90.0000	47.5000	1.9104	431.8	431.8	38.1	103.1507	0.2390	14.042	0.0325	0.09	423.1	0.464E-04
6	4	10.0000	52.4000	2.1879	1023.5	1023.5	65.4	105.2207	0.2438	83.657	0.1938	0.11	773.2	0.545E-04
7	5	30.0000	29.9000	2.1283	1017.0	1016.9	141.8	72.4972	0.1679	57.636	0.1335	0.23	773.1	0.755E-04
8	7	20.0000	26.4000	1.9679	1022.7	1022.5	89.3	32.7870	0.0760	26.061	0.0604	0.14	773.2	0.348E-04
9	8	0.0000	52.0000	1.0056	776.6	776.2	134.9	129.3224	0.2996	66.651	0.1544	0.25	573.1	0.246E-03
10	8	85.0000	62.2895	1.0285	778.8	778.8	91.6	128.2737	0.2972	65.849	0.1525	0.17	573.1	0.230E-03
11	11	280.0000	62.0000	0.9520	292.4	292.4	39.5	134.9684	0.3127	-0.675	-0.0016	0.12	313.1	0.326E-03
12	9	20.0000	50.0000	1.9128	431.8	431.8	34.1	103.2943	0.2393	14.007	0.0324	0.08	433.1	0.210E-04
13	10	280.0000	53.0000	2.1887	1023.8	1023.8	63.9	105.1678	0.2436	83.639	0.1938	0.10	1023.2	0.513E-04
14	12	20.0000	63.5000	1.0304	775.8	775.7	87.2	127.9826	0.2965	65.156	0.1509	0.16	298.0	0.201E-03
15	12	380.0000	63.5000	1.0319	754.4	754.5	79.2	119.6458	0.2772	58.071	0.1345	0.15	298.0	0.797E-04

3.9 RESULTS

The summarized results of the experimental research on the virtual test rig are presented in Table 5.7, representing both the values of pressures, temperatures, flow rates of high-pressure exhaust gases HPG and fresh air LPA (the input data of the simulations) as well as the obtained values of the same fluid parameters, respectively HPA compressed air and LPG low pressure gases. The table also shows the values resulting from the third simulation performed for the comparison of the values with the data from the literature, where the relative errors between the simulation results reported to the experimental ones, reported by Smith [57] and Pohorelsky et al., were also calculated [47].

It can be observed that, in terms of the HPG pressure, a stabilized value of 2.18 bar was recorded, comparable to those reported experimentally, of 2.1...2.25 bar. The calculated relative error is a minimum of 3.1 % and a maximum of 10 %, the latter being related to the experimental data obtained with no set temperature [57]. Regarding the output data in simulation 3, a HPA air pressure of 1.91 bar was obtained, comparable to the experimental literature data of 1.95 or 2.05 bar. A significant difference is recorded in the compressed air flow values, where the PWSMG delivers 19...20 % higher flows, the explanation being that in the design of the new PWSMG one of the imposed conditions was the delivery of increased compressed air flows, so that, by imposing in the input data gas flow values equal to the CX-93, the PWSMG transferred this flow to the compressed air with no additional loss in the LPG port. It is also observed that the fresh air and exhaust gas flow rates have close values, which means that part of the air

drawn into the PWSMG goes directly to the exhaust port, thus "washing" the remaining gas channels and cooling the hot part of the PWSMG.

Table 5.7 – Parameters of working fluids obtained experimentally from specialized literature, the parameters obtained in the experimental research in a virtual environment for the new pressure wave supercharger and the relative errors compared to the experimental values

Experimental data reported in literature				
	Pohorelsky et al.[47]-1			
Parameters	HPG	HPA	LPG	LPA
Pression [bar]	2,25	2,05	1,06	1,003
Temp. [K]	900	393	600	400
Mass flow [g/s]	100	83,3	150	147

	Pohorelsky et al.[47]-2			
Parameters	HPG	HPA	LPG	LPA
Pression [bar]	2,1	1,95	1	1,003
Temp. [K]	900	400	595	393
Mass flow [g/s]	100	83,3	147	147

	Smith [54]			
Parameters	HPG	HPA	LPG	LPA
Pression [bar]	1,978	1,6	1,06	1
Temp. [K]	498	402	426	318
Mass flow [g/s]	99,34	87	88,5	73,4

Simulation results for PWSMG				
	Virtual model AVL Boost PWSGM simulation 3			
Parameters	HPG	HPA	LPG	LPA
Pression [bar]	2,18	1,91	1,028	0,95
Temp. [K]	1023	431,8	776,8	292
Mass flow [g/s]	103,22	103,5	128	133,2

	Virtual model AVL Boost PWSGM simulation 2			
Parameters	HPG	HPA	LPG	LPA
Pression [bar]	2,068	1,94	1,03	0,925
Temp. [K]	1023	410	690	290
Mass flow [g/s]	162	159,7	256	253

	Virtual model AVL Boost PWSGM simulation 1			
Parameters	HPG	HPA	LPG	LPA
Pression [bar]	2,43	2,38	1,014	0,95
Temp. [K]	1023	570	853	294
Mass flow [g/s]	140	142,9	120	117

Relative errors [%]				
	Simulare 3 vs.Pohorelsky [47]-1			
Parameters	HPG	HPA	LPG	LPA
Pression [bar]	3,1	6,8	3,0	5,3
Temp. [K]	-13,7	-9,9	-29,5	27,0
Mass flow [g/s]	-3,2	-24,2	14,7	9,4

	Simulare 3 vs.Pohorelsky[47]-2			
Parameters	HPG	HPA	LPG	LPA
Pression [bar]	-3,8	2,1	-2,5	5,3
Temp. [K]	-13,7	-8,0	-30,6	25,7
Mass flow [g/s]	-3,2	-24,2	12,9	9,4

	Simulare 3 vs. Smith [54]			
Parameters	HPG	HPA	LPG	LPA
Pression [bar]	-10,2	-19,4	3,0	5,3
Temp. [K]	-105,4	-7,4	-82,3	8,2
Mass flow [g/s]	-3,9	-19,0	-44,6	-81,5

Simulations 1 and 2 were performed in order to analyze the operation of the PWSMG when supercharging the symbolic M6000 engine. Simulation 1 was performed imposing an exhaust gas pressure of ~2.4 bar and inlet flow rates ~50% higher compared to the CX-93, and for simulation 2 a pressure of 2.1 bar and flow rates also increased by 50%, to observe the operation of the PWSMG when supercharging engines discharging at higher pressures and temperatures. Thus, the compressed air pressure recorded values of 2.38 bar, respectively 1.94 bar, and the compressed air flow rates of 159 g/s, respectively 143 g/s for the two simulations. In terms of temperature values in the ports, a ratio of 1.2 was set between the simulation exhaust gas temperatures vs. actual experimental values (M-6000 engine modeling condition). For the 2nd simulation, at similar values of exhaust gas inlet pressure and compressed air pressure, the fluid temperatures have close values, but the PWSMG can "process" ~50% higher flow rates, so as established for the hypothetical M-6000 engine. Also, for higher gas inlet pressures and for resulted compressed air pressures in relation to approx. 2,3, the flow rates of HPG and HPA are ~ 1.4 higher than CX-93 flow rates, also falling within the range of 1...1.5 proposed in the research hypotheses. In conclusion, the obtained data validate the PWSMG model with the proposed geometric configuration and the assumptions established for modeling.

3.10 THE MECHANICAL WORK PULLED OUT TO THE PWSMG SHAFT

Starting from the idea of a difference between the tangential component of the speed in the ports and the peripheral one of the rotor, and keeping the condition of the optimal speed of the rotor, an impulse in the rotor resulted in the production of power, so that the PWSMG will create useful mechanical work on the shaft. It can be calculated according to the axial moment exerted on the shaft in the direction of rotation, Ma [102]:

$$\dot{W}_{SUPGM} = M_a\omega = (V_T \cdot V_{s1} - V_T \cdot V_{s2})\dot{m}_a + (V_T \cdot V_{s3} - V_T \cdot V_{s4})\dot{m}_g \quad (5.2)$$

where $\dot{m}_a$ and $\dot{m}_g$ are the air, respectively burnt gases flows, and Vsi are the tangential components of the velocities (Fig. 5.28). Substituting from the velocity diagram the flow rates according to the stagnation densities, provided that the velocities w relative to the rotor are equal: w1≈w4 and w2≈w3, then the energy flow extracted will be:

$$\dot{W}_{SUPGM} = V_T \sin\beta\,(w_2 - w_1)\dot{m}_a \cdot \left(1 - \frac{\rho_{0g}}{\rho_{0a}}\right) \quad (5.5)$$

It can be seen that, if β=0, no mechanical work can be extracted, the supercharger being only a pressure exchanger. In Table 5.8 the values for $\dot{W}_{SUPGM}$ are calculated. These values are relatively small and possibly cover the driving power requirement, but if it is taken into account that in real operating conditions the engine of a vehicle develops net higher state parameters, it can be expected that this energy can become an additional source of energy required on board of a vehicle with a conventional or hybrid propulsion system.

*Table 5.8. Energy extracted during PWS operation in two cases considered (*SUPGM = PWSMG)*

	SUPGM 1	SUPGM 2
V_T [m/s]	97	97
w1 [m/s]	27,467989	27,467989
w2 [m/s]	226,10306	226,10306
ρ0g/ρ0a	0,5865385	0,6093023
W_SUPGM [W]	**165,19784**	**156,10258**

3.11 NOISE

The frequency of the sound produced by the PWS can be calculated with [27]:

$$f = \frac{i \cdot z \cdot n}{60}\ [Hz] \quad (5.6)$$

where : i – number of rows, z – number of channels, n – rotor speed.

For the CX-93, at optimal speeds of 2500...15000 rpm, the sound frequency is between 1400...8500 Hz, which makes the noise produced completely in the audible zone. For a high speed range,

for PWSMG of 10,000...22,500 rpm, with 2 or 3 rows of channels and 36 channels, the sound frequency will be in the area: 12,000...27,000 Hz, or 18,000... 40,500 Hz. As the area perceptible to the human ear is up to 20,000 Hz, the PWSMG can become silent at revs above 16500 rpm.

3.12 ENERGY TRANSFER PERFORMANCE

The efficiency with which the energy contained in the combustion gases is transferred to the intake air can be calculated as the ratio of the increase in the mechanical work of expanding the gases, which could ideally be extracted and transmitted to the air, and the mechanical work contained in the exhaust gases [102]:

$$\eta_E = \frac{\dot{W}_{HPA} - \dot{W}_{LPA}}{\dot{W}_{HPG}} \qquad (5.7)$$

where $\dot{W}_i$ is the energy flow that can be generated by expanding a gas from a defined state to a reference state (considered the ambient pressure p_A):

$$\dot{W}_i = \dot{m}_i \cdot c_{pi} \cdot T_i \left[1 - \left(\frac{p_A}{p_{0i}}\right)^{\frac{k-1}{k}}\right] \qquad (5.8)$$

p_{0i} – the stagnation pressure of the respective fluid. The calculated values of $\dot{W}_i$ and η_E for the originally estimated data sets for PWSMG shows that the CX efficiency is ~64 %, and for PWSMG, the average efficiency would be ~67%, when the working pressures and temperatures are clearly higher than those of CX-93. It can also be observed, taking into account the significant influence of the temperature of the exhaust gases in the operation of the PWS, that at similar temperatures the energy transfer efficiency of the PWSMG is 70%, under the conditions of a compressed air pressure at the PWSMG that is higher than that obtained at the CX- 93.

CHAPTER 4| FINAL CONCLUSIONS. ORIGINAL CONTRIBUTIONS.

4.1 FINAL CONCLUSIONS

Equipments using pressure wave technology have been studied for decades, especially since the second half of the last century, showing interest especially in the aeronautical industry, with applications in the improvement of gas turbines or shock wave engines, but also in industry cars, as superchargers for internal combustion engines. The challenges in stating as rigorously as possible the theoretical equations that describe the behavior of fluids, in establishing new configurations and geometrical adjustments or new and reliable materials for pressure wave superchargers have been overcome by developing computational, modeling and simulation codes, the work of researchers improving significantly, the errors between the experimental values and those in the virtual environment being reduced.

The present work approached the topic of optimizing the configuration and geometric shapes of the pressure wave supercharger, choosing as a base model the Comprex CX-93, the most successful PWS, installed with very good results on more than 150,000 vehicles in series production. The proposed objectives were achieved through:

1. **Improving the geometric and constructive dimensions of the rotor,** increasing the number of channels and/or the number of rows of channels, the axial inclination of the channels, the reduction of the length of the rotor from 93 mm (CX-93) to 58 mm;
2. **Redesigning a new supercharger**, named simbollicaly **PWSMG,** having 72 cells, arranged radially on 2 or 3 rows of channels, having channel sections of different shapes - the 3 types of geometries each have their own advantages. Optimization had the main target:
3. **Extending the range of applicability of the new supercharger** to engines in accordance with current trends in the automotive industry (reduced emissions, downsizing, elimination of diesel engines, use of alternative or low-carbon fuels). The new PWSMG has the potential to supercharge a wide range of engines that require increased intake air flow, or run on a fuel that provides higher exhaust gas pressures and temperatures, or have higher rated engine speeds than the diesel engine. reference.
4. **Supply of additional energy** which allows the use of PWSMG in hybrid mode, both as a pressure exchanger (specific conventional PWS) and in turbine mode.
5. **Maintaining the energy transfer efficiency value** of the new supercharger compared to the CX-93 supercharger.
6. **Noise reduction**, estimated to be achieved by increasing the number of channels, possibly the number of rows of channels and the row's shift and, last but not least, by increasing the rotor speed, a consequence of the use in applications with higher state parameters.

The modeling and simulation in the virtual environment was done in two stages: initially the operation of the CX-93 was simulated on the AVL Boost virtual stand, followed by the validation of the model and its use as a tool for the simulation on the AVL Boost virtual stand of the operation of the new PWS with modified geometry. The results obtained demonstrated that this new supercharger has the ability to supercharge engines with higher operating parameters compared to the reference diesel engine and to provide increased supercharging pressure ratios, has an energy transfer efficiency as good as the CX-93, has the ability to provide mechanical work to the shaft which, in real conditions and with appropriate adjustments, can become an additional source of energy on the board of vehicles.

4.2 PERSONAL CONTRIBUTIONS

The theoretical and experimental activities in a virtual environment carried out and detailed in this paper have generated a series of personal contributions to the development of the pressure wave compressor, with the possibility of its realization and implementation on a range of applications. The main contribution lies in the **realization of a new geometry** for the pressure wave supercharger which:

- operates hybridly, both as a supercharger and as a turbine, with a better energy transfer efficiency and allowing mechanical work to be pulled out at the rotor shaft;

- is capable of being used on several types of engines, with superior characteristics to the diesel engine for which it was originally created and improved, targeting hydrogen or natural gas engines;

- can be physically made and easily implemented, by keeping the position and shape of the covers of the conventional CX-93 supercharger, with small changes in curvature of the side walls of the ports and pockets;

- allows the reduction of the global dimensions, by reducing the length of the rotor;

- produces a diminished noise compared to the conventional CX.

To achieve the proposed objectives, theoretical calculation models with personal contribution were used, as follows:

- **mathematical models for calculating the channel section and the number of channels**, used in determining the geometric configuration of the PWSMG rotor variants – by approximating the length of the arcs with the distance between their end points (variant 2) and imposing a surface utilization efficiency (variants 2 and 3) and imposing the condition of keeping the minimum thickness of canal walls;

- **mathematical model for calculating pressure losses given by local resistances or by friction**, by considering simplified aeraulic circuits, in which it is possible to apply established formulas for flow over rough surfaces, with local losses in section changes, narrowings or sudden openings, deviation from the flow direction or fluid return, ramifications, etc.

- model for calculating the angle of inclination of the channels, depending on the operating parameters of the symbolic engine M6000;

- calculation model for determining the critical surface and the maximum flow rate by making an analogy between the flow type at the opening of the channels in front of the ports and the flow in the convergent-divergent nozzles, thus allowing the calculation of the critical section, respectively the calculation of the maximum flow rate in the section of the rotor channel.

The present paper brings back in foreground and highlights the potential of the pressure wave compressor, equipment successfully used in supercharging internal combustion engines several decades ago and recently revived by the company currently holding the Comprex patent. Extending the use of PWS from diesel engines, engines on which it was predominantly used, to "modern", faster and/or small displacement engines, was one of the targets of this work, for which a design reconfiguration of the pressure wave supercharger rotor was carried out, with the achievement of other advantages such as useful mechanical work on the rotor shaft and reduced noise. The new PWS can be easily realized physically by using modern technological processes, being small in size and having geometric shapes that are easy to process mechanically. The choice of new materials with improved mechanical and thermal qualities are some of the future research directions.

REFERENCES

[1] https://www.britannica.com/biography/Jean-de-Hautefeuille

[2] https://fr.wikipedia.org/wiki/Jean_de_Hautefeuille#cite_note-5

[3] Buchanan, Robert Angus. "history of technology". Encyclopedia Britannica, Revizuit 18 Nov. 2020, https://www.britannica.com/technology/history-of-technology .

[4] https://en.wikipedia.org/wiki/Internal_combustion_engine

[5] https://ec.europa.eu/clima/eu-action/climate-strategies-targets/2030-climate-energy-framework_en

[6] http://www.eea.europa.eu/EEA , 2015, Monitoring CO2 emissions from new passenger cars and vans in 2014. EEA Technical report No 16/2015, European Environment Agency. Accesat Aprilie 2022

[7] www.statista.com

[8] https://www.oica.net/category/production-statistics/2021-statistics/

[9] Regulation (EC) No 443/2009 of the European Parliament and of the Council of 23 April 2009 setting emission performance standards for new passenger cars as part of the Community's integrated approach to reduce CO2 emissions from light-duty vehicles, OJL140, http://ec.europa.eu/clima/policies/transport/vehicles/cars/indexen.htm

[10] Tsiakmakis, S., Ciuffo, B., Fontaras, G., Cubito, C., Pavlovic, J. , Anagnostopoulos, K., From NEDC to WLTP: effect on the type-approval CO_2 emissions of light-duty vehicles, EUR 28724 EN, Publications Office of the European Union, Luxembourg, 2017, ISBN 978-92-79-71642-3, https://doi.org/10.2760/93419 , JRC107662.

[11] Liu, X.; Zhao, F.; Hao, H.; Chen, K.; Liu, Z.; Babiker, H.; Amer, A.A. From NEDC to WLTP: Effect on the Energy Consumption, NEV Credits, and Subsidies Policies of PHEV in the Chinese Market. Sustainability 2020, 12, 5747. https://doi.org/10.3390/su12145747

[12] Horizon 2020 – EU.3.4.- Societal Challenges - Smart, Green And Integrated Transport, https://cordis.europa.eu/programme/id/H2020-EU.3.4.

[13] Regulation (EU) 2019/1242 of the European Parliament and of the Council of 20 June 2019 setting CO_2 emission performance standards for new heavy-duty vehicles and amending Regulations (EC) No 595/2009 and (EU) 2018/956 of the European Parliament and of the Council and Council Directive 96/53/EC, July 2019, https://eur-lex.europa.eu/eli/reg/2019/1242/oj

[14] Delgado, O., Rodriguez, F., Muncrief, R., "Fuel efficiency technology in European heavy-duty vehicles: baseline and potential for the 2020–2030 timeframe", The International Council on Clean Transportation, 2017

[15] **Costiuc, I.;** Chiru, A.; Costiuc, L. Pressure Wave Technology - An interesting approach in SUPercharging, *Rom. J. Tech. Sci. Appl. Mech.* 2018, 63, 50–73. Recent Research Advances in Automotive Engineering; Romanian Academy Publishing House, 2018

[16] Rajput, R.K., A Textbook Of Internal Combustion Engines, by Laxmi Publications (P) Ltd., Third Edition : 2016, ISBN 81-318-0066-0

[17] **Costiuc, I.,** Chiru, A. "Modelarea proceselor termodinamice în compresoarele cu unde de presiune", Revista Industria Automobilului Nr.43/Iunie 2017, Romanian Journal of Automotive Engineering, RoJAE 23(2) 49 – 90 (2017), ISSN 2457 – 5275

[18] Hasler, C., Designing a bespoke high efficiency turbine stage for a key engine condition through pulse utilization, Turbochargers and Turbocharging XIV – Institution of Mechanical Engineers, CRC Press, Taylor & Francis, ISBN: 978-0-367-67645-2, LONDON, UK, 2021

[19] Heisler, H., Advances Engine Technology, SAE International, 1995, ISBN 1 56091 734 2.

[20] **Costiuc** I., Costiuc L., "Numerical Investigation of a Pressure Wave SUPercharger", 31st International Congress AITS Chişinău, Rep.Moldova (2021), 2022 IOP Conf. Ser.: Mater. Sci. Eng. 1220 012022, doi:10.1088/1757-899X/1220/1/012022

[21] Hiereth, H.; Prenninger, H. Aufladung der Verbrennungskraftmaschine; Springer: Vienna, Austria, 2003; ISSN 1613-6349

[22] **Costiuc**, I., Chiru, A., Evolution of the Pressure Wave SUPercharger Concept, 2017 IOP Conf. Series: Materials Science and Engineering, Vol. 252, 012081, 2017

[23] Petitt, J., Sport Compact Turbos & Blowers, CarTech Inc, ISBN 1884089887, 2004

[24] Georgano, G.N. The new encyclopedia of motorcars 1885 to the present (ed.3. ed.), New York: Dutton. p. 415. ISBN 0-525-93254-2, 1992

[25] Azoury, P.H., An Introduction to the Dynamic Pressure Exchanger, Proceedings of the Institution of Mechanical Engineers, Vol 180, Issue 1, pp. 451 – 480, 1965-66

[26] Knauff, R., 1906, "Converting Pressures of Liberated Gas Energy into Mechanical Work," British Patent 2818

[27] Pranav, A.S., Wave Rotor Test Rig Design Procedure for Gas Turbine Enhancement, Michigan State University. Department of Mechanical Engineering, 2008

[28] Lebre, A. F. British Patent No. 290 669, 1928

[29] Burghard, H. German Patent No. 485 386,1928

[30] Berchtold, M., "The Comprex Diesel SUPercharger", SAE Paper 590001, Vol.67, 1959

[31] Akbari, P., Nalim, R., Mueller, N. – A Review of Wave Rotor Technology and its Applications. Journal of Engineering for Gas Turbines and Power, Vol.128, Oct.2006.

[32] Zehnder, G., Mayer, A., Mathews, L., The Free Running Comprex®, SAE Paper 890452, 1989

[33] Taussig, R.T., Hertzberg, A., "Wave Rotors for Turbomachinery", Winter Annual Meeting of the ASME, Machinery for Direct Fluid-Fluid Energy Exchange, edited by J. F. Sladky, AD-07, pp. 1–7., 1984

[34] Spring, P., "Modeling and Control of Pressure-Wave SUPercharged Engine Systems", PhD Diss. ETH Zurich, 2006

[35] **Costiuc**, I.; Chiru, A.; Costiuc, L. A Review of Engine's Performance When SUPercharging by a Pressure Wave SUPercharger. *Energies 2022*, 15, 2721. https://doi.org/10.3390/en15082721

[36] Thayer, W. J., "The MSNW Energy Exchanger Research Program," Proceedings ONR/NAVAIR Wave Rotor Research and Technology Workshop, Naval Postgraduate School, Monterey, CA, Report NPS-67-85-008, 1985

[37] Mathur, A., "Design and Experimental Verification of Wave Rotor Cycles," Proceedings ONR/NAVAIR Wave Rotor Research and Technology Workshop, Naval Postgraduate School, Monterey, CA, Report NPS-67-85- 008, 1985

[38] Mathur, A., "Wave Rotor Research: A Computer Code for Preliminary Design of Wave Diagrams," Naval Postgraduate School, Monterey, CA, Report NPS67-85-006CR, 1985

[39] Eidelman, S., "Gradual Opening of Rectangular and Skewed Wave Rotor Passages," Proceedings ONR/NAVAIR Wave Rotor Research and Technology Workshop, Naval Postgraduate School, Monterey, CA, NPS- 67-85-008, 1985

[40] Nalim, M.R.A.Z.I.; Nalim, M. Numerical Study of Stratified Charge Combustion in Wave Rotors. In Proceedings of the 33rd Joint Propulsion Conference and Exhibit, Seattle, WA, USA, 6–9 July 1997

[41] Soltic, P. Part-Load Optimized SI Engine Systems. Ph.D. Thesis, ETH Zurich, Switzerland, 2001

[42] Frackowiak, M.; Iancu, F.; Potrzebowski, A.; Akbari, P.; Müller, N.; Piechna, J. Numerical Simulation of Unsteady-Flow Processes in Wave Rotors. In Proceedings of the IMECE04 2004 ASME International Mechanical Engineering Congress, Anaheim, CA, USA, IMECE2004-60973, 13–19 Nov. 2004

[43] Fatsis, A.; Ribaud, Y. Numerical Analysis of the Unsteady Flow InsideWave Rotors Applied to Air Breathing Engines. Proceedings of the 13th International Symposium on Air-breathing Engines, Chattanooga, TN, USA, 1997. Paper ISABE-97-7214, 1997

[44] Fatsis, A.; Ribaud, Y. Preliminary Analysis of the Flow inside a Three-Port Wave Rotor by Means of a Numerical Model. Aerosp. Sci. Technol., 2, 289–300, 1998

[45] Okamoto, K.; Nagashima, T.; Yamaguchi, K. Rotor-Wall Clearance Effects upon Wave Rotor Passage Flow. Proceedings of 15th International Symp. on Airbreathing Engines, Bangalore, India, 2001. Paper ISABE-2001-1222.

[46] Okamoto, K.; Nagashima, T. A Simple Numerical Approach of Micro Wave Rotor Gasdynamic Design. In Proceedings of 16th International Symposium on Airbreathing Engines, Cleveland, OH, USA, 2003. ISABE-1213.

[47] Podhorelsky, L.; Macek, J.; Polasek, M.; Vitek, O. Simulation of a Comprex Pressure Exchanger in 1-D Code; SAE Paper 04P-241; SAE: Warrendale, PA, USA, 2004.

[48] Binder, E. Untersuchungen zum Potential eines Verbrennungsmotors mit Druckwellenlader. Ph.D. Thesis, Technical University of Braunschweig, Braunschweig, Germany, ISSN 2199-708X. 2015

[49] Basu, S. One-Dimensional Simulation of Non-Steady Channel Flow in a Pressure-Wave SUPercharger with a Pocket. MS Thesis at Combustion and Propulsion Research Lab, Purdue School of Engineering and Technology, Indianapolis, IN, USA. Unpublished MS Project Report. 2018

[50] Basu, S.; Comparison of Versions of One-Dimensional Program to Simulate Non-Steady Flow in a Pressure-Wave SUPercharger with Pockets. Combustion and Propulsion Research Lab, Purdue School of Engineering and Technology, Indianapolis, IN, USA, 2018

[51] Sutar, P. Numerical Simulation of Pressure Wave SUPercharger with Pockets Operating at Different Speeds. Master's Thesis, Purdue University, West Lafayette, IN, USA, 2020.

[52] Available online: http://www.swissauto.com (accessed on 17 January 2022).

[53] Guzella, L., Martin, R.; The SAVE engine concept, Ch. "New Engines". MTZ-Mot. Z. 59, 1998

[54] Smith, B.D. Scaling Study of Wave Rotor Turbo-Normalization of A Small Internal Combustion Engine. Master's Thesis, Air Force Institute of Technology, Dayton, OH, USA, 2012. https://scholar.afit.edu/etd/1066/

[55] Mataczynski, M.R., Design and Simulation of a Pressure Wave SUPercharger for a Small Two-Stroke Engine. Ph.D. Thesis, Air Force Institute of Technology, Wright-Patterson Air Force Base, Dayton, OH, USA, 2014.

[56] Beasley, B.A., Investigation of a Pressure Wave SUPercharger for an Industrial Diesel Engine. Ph.D. Thesis, Air Force Institute of Technology, Wright-Patterson Air Force Base, Dayton, OH, USA, 2018.

[57] Antrova, A.G. Pressure Wave SUPercharger. U.S. Patent US 2017/0211464 A1, 27 July 2017.

[58] Zsiga, N.; Skopil, M.A.; Wang, M.; Klein, D.; Soltic, P.; Comparison of Turbocharging and Pressure Wave SUPercharging of a Natural Gas Engine for Light Commercial Trucks and Vans. Energies 2021, 14, 5306.

[59] Skopil, M.A. Wasserstoff Motoren und das neue Comprex™ Druckwellenlader Konzept. Proceedings of the 42nd International Vienna Motor Symposium, Vienna, Austria, 29–30 April 2021.

[60] https://www.admin.ch/gov/de/start/dokumentation/medienmitteilungen.msg-id-87724.html

[61] Weber, H.E., Shock Wave Engine Design, John Wiley & Sons Inc., N.Y., ISBN 0-471-59724-4, 1995

[62] Doerfler, P., "Comprex SUPercharging of Vehicle Diesel Engines," SAE Technical Paper 750335, 1975, doi: 10.4271/750335.

[63] Heywood, J.; Internal Combustion Engine Fundamentals, McGraw-Hill International Editions, II. Series, 1988.

[64] Gyarmathy, G., 1983, "How Does the Comprex® Pressure-Wave SUPercharger Work?," SAE Paper 830234, International Congress and Exposition, Detroit, Michigan, 1983.

[65] Berchtold, M.; SUPercharging with Comprex, Proceedings of ONR/NAVAIR Wave Rotor Research and Technology Workshop, Naval Postgraduate School, Monterey, CA, Report NPS-67-85-008, pp. 51–74, 1985
[66] Kentfield, J.A.C.; The Pressure Exchanger: An Introduction Including a Review of the Work of Power Jets (R&D) Ltd., Proceedings ONR/NAVAIR Wave Rotor Research and Technology Workshop, Naval Postgraduate School, Monterey, CA, Report NPS- 67-85-008, pp. 9-50, 1985
[67] Pischinger, S. Verbrennungskraftmaschinen II, VK II Lecture notes, RWTH Aachen University, 1984.
[68] Berchtold, M.; Gull, H.P. Road Performance of a Comprex SUPercharged Diesel Truck. SAE Trans. 1960.
[69] Berchtold, M.; Pressure wave charging for small vehicle diesel engines. Schweiz. Bauztg. 1961, 46, 801–809.
[70] Wunsch, A.; Charging vehicle diesel engines with the exhaust gas turbocharger and the Comprex pressure wave machine. Mot. Z. 1990, 1, 19.
[71] Gygax, J.; Schneider, G. Operating experiences with the Comprex pressure wave SUPercharger in the Opel Senator. MTZ-Mot. Z. 1988, 9, 335–340.
[72] Weaving, J.H. Internal Combustion Engineering, Science and Technology; Elsevier Science Publishers Ltd.: Dordrecht, The Netherlands, 1990; ISBN 978-94-010-6822-2.
[73] Zehnder, G.W.; Mayer, A. Comprex® Pressure-Wave SUPercharging for Automotive Diesels-State-of-the-Art. SAE Trans. 1984, 93, 756–771.
[74] Schruf, G.M.; Kollbrunner, T.A. Application and Matching of the Comprex Pressure-Wave SUPercharger to Automotive Diesel Engines; SAE Technical paper 840133; SAE:Warrendale, PA, USA, 1985; ISSN 0148-7191
[75] Leahu, C.; Optimisation of Compression Ignition Engine using SUPercharging Systems. Ph.D. Thesis, University Transilvania Brasov, Brasov, Romania, 2011
[76] Kollbrunner, T.A. Comprex SUPercharging for Passenger Diesel Car Engines; SAE Paper 800884; SAE: Warrendale, PA, USA, 1981; ISSN 0148-7191.
[77] Mayer, A.; Oda, J.; Kato, K.; Haase, W.; Fried, R.; Extruded Ceramic—A New Technology for the Comprex Rotor; SAE Technical Paper 890425; SAE:Warrendale, PA, USA, 1989.
[78] Hiereth, H. Daimler-Benz AG—Car Tests with a Free-Running Pressure-Wave Charger—A Study for an Advanced SUPercharging System; SAE Technical Paper 890453; SAE: Warrendale, PA, USA, 1989.
[79] Tatsutomi, Y.; Yoshizu, K.; Komagamine, M. The diesel engine with Comprex charging for the Mazda 626. Mot. Z. 1990, 51, 126.
[80] Walzer, P.; Emmenthal, K.D.; Rottenkolbe, P. Charging Systems for Passenger Car Drives; Automobil Industrie: Würzburg, Germany, 1989.
[81] Wiedemann, B.; Rhode, W. The Behavior of Different SUPercharging Systems on Fast-Reviving Diesel Engines. Available online: https://publications.rwth-aachen.de/record/824367 (accessed on 17 January 2022).
[82] Hiereth, H. Assessment of the Suitability of New SUPercharging Systems for Vehicle Engines. Available online: https://publications.rwth-aachen.de/record/824367.
[83] https://www.formulapassion.it/motorsport/storia/f1-ferrari-comprex-1981
[84] Flückiger, L.; Tafel, S.; Spring, P. SUPercharging with pressure wave SUPercharger for petrol engines. MTZ-Mot. Z. 2006, 67, 946–954.
[85] Lei, Y.; Zhou, D.S.; Zhang, H.G. Investigation on performance of a compression-ignition engine with pressure-wave SUPercharger. Energy 2010, 35, 85–93
[86] Radu, G.A.; Leahu, C.I. Alternative Solution for SUPercharging with Aggregates of Turbocharger Type. Eng. Sci. 2011, 4, 14–18.

[87] Atanasiu, C.G. Researches Regarding Automobile Engine's SUPercharging. Ph.D. Thesis, University Transilvania of Brasov, Brasov, Romania, 2013

[88] Environmental Protection Agency Test Results on a Mercedes-Benz 220D Diesel Sedan Equipped with a Comprex Pressure-Wave SUPercharger; Technical Report NP-1902429; Environmental Protection Agency–Technology Assessment and Evaluation Branch: Ann Arbor, MI, USA, 1975.

[89] Barth, E.A.; Burgeson, R.N.; Emissions and Fuel Economy of a Comprex Pressure Wave SUPercharged Diesel, Test and Evaluation Branch, Emission Control Technology Division Office of Mobile Source Air Pollution Control Office of Air, Noise and Radiation Environmental Protection Agency; Technical Report; Environmental Protection Agency: Ann Arbor, MI, USA, 1980.

[90] Amstutz, A. Geregelte Exhaust Gas Recirculation to Reduce Nitrogen Oxide and Particle Emissions in Diesel Engines with Comprex Charging. Ph.D. Thesis, ETH Zurich, Switzerland, 1990.

[91] Jonsson, V. K., Mathews, L., Spalding, D. B. – Numerical Solution Procedure for Calculating the Un-steady, One – Dimensional Floe of Compressible Fluid, ASME Paper 73-FE-30, 1973

[92] Fu, J, Liu, J., Wang, Y., Deng, B., Yang, Y., Feng, R., Yang, J.: A comparative study on various turbocharging approaches based on IC engine exhaust gas energy recovery, Applied Energy 113, 2014

[93] Skopil, M.A., Ein neues Druckwellenladerkonzept für weniger Emissionen und mehr Effizienz, www.antrova.ch

[94] Weber H.E., Wave Engine Aerothermodynamic Design, Transactions of the ASME, Journal of Engineering for Gas Turbines and Power, OCTOBER 1992, Vol.114, pp.790-796.

[95] Recknagel, Sprenger, Schramek; Taschenbuch für Heizung und Klimatechnik 2009/2010, Publisher: 2009 Oldenbourg Industrieverlag GmbH, ISBN 978-3-8356-3134-2

[96] Hitomi, Yuzuriha, Y., Tanaka, K., The Cha.racteristics of Pressure Wave SUPercharged Small Diesel Engine, SAE Paper 890454, 1989

[97] Anderson, J.D Jr, Fundamentals of Aerodynamics, ed.5, McGraw-Hill, 2011

[98] Powers, J.M. - Lecture notes on gas dynamics. University of Notre Dame, USA, 2015.

[99] Çengel, Y.A.,Boles, M.A., Kanoğlu, M., Thermodynamics : an engineering approach / Ninth edition. New York, NY : McGraw-Hill Education, 2019, ISBN 978-1-259-82267-4

[100] Akbari, P.; Mueller, N.; Gas Dynamic design Analyses of Charging Zone for Reverse-Flow Pressure Wave SUPerchargers. In: Spring Technical Conference of the ASME Internal Combustion Engine Division, Salzburg, 2003

[101] Arjanikov, N.S., Malțev, V.N., Aerodinamica, Ed.Tehnică, 1954

[102] Taussig, R., Cassady, P., Oates, G., Investigation of Wave rotor for Cruise Engines, U.S.NAP Center, Vol.2, 1983

[103] Walner, T., Luhse-Busch, H., Performance, Efficiency, and Emissions Evaluation of a SUPercharged Hydrogen-Powered, 4-Cylinder Engine, Fuels & Emissions Conference Cape Town, South Africa, 2007, SAE Paper 2007-01-0016

[104] Lilik, G.K., Hydrogen Assisted Diesel Combustion, PhD Thesis, Pennsylvania State University, 2008

[105] Thyer, U., 1,6 Litre SUPercharged CNG Engine, AutoTechnology, Nr. 4, 2007

[106] Shreeve, R., Mathur, A., Eidelman, S., Erwin, J., Wave Rotor Technology Status and Research Progress, Naval Postgraduate School, Monterey, California, NPS67, 1982.

[107] Costiuc I., Costiuc L., Chiru A. "Investigation of pressure field along the channel of a Pressure Wave SUPercharger", The 31st International Congress AITS Chişinău, Rep.Moldova (2021) 2022 IOP Conf. Ser.: Mater. Sci. Eng. 1220 012023, doi:10.1088/1757-899X/1220/1/012023